

## APPLIED SCIENCES AND ENGINEERING

# Injectable shear-thinning hydrogels promote oligodendrocyte progenitor cell survival and remyelination in the central nervous system

Ashis Kumar Podder<sup>1†</sup>, Mohamed Alaa Mohamed<sup>1†‡</sup>, Richard A. Seidman<sup>2</sup>, Georgios Tseropoulos<sup>1§</sup>, Jessie J. Polanco<sup>3</sup>, Pedro Lei<sup>1</sup>, Fraser J. Sim<sup>2,3\*</sup>, Stelios T. Andreadis<sup>1,4,5,6\*</sup>

Cell therapy for the treatment of demyelinating diseases such as multiple sclerosis is hampered by poor survival of donor oligodendrocyte cell preparations, resulting in limited therapeutic outcomes. Excessive cell death leads to the release of intracellular alloantigens, which likely exacerbate local inflammation and may predispose the graft to eventual rejection. Here, we engineered innovative cell-instructive shear-thinning hydrogels (STHs) with tunable viscoelasticity and bioactivity for minimally invasive delivery of primary human oligodendrocyte progenitor cells (hOPCs) to the brain of a *shiverer/rag2* mouse, a model of congenital hypomyelinating disease. The STHs enabled immobilization of pro-survival signals, including a recombinantly designed bidomain peptide and platelet-derived growth factor. Notably, STHs reduced the death rate of hOPCs significantly, promoted the production of myelinating oligodendrocytes, and enhanced myelination of the mouse brain 12 weeks post-implantation. Our results demonstrate the potential of STHs loaded with biological cues to improve cell therapies for the treatment of devastating myelopathies.

## INTRODUCTION

In demyelinating diseases such as multiple sclerosis, the inflammatory tissue environment in chronic lesions prevents efficient progenitor recruitment, leading to failure in oligodendrocyte regeneration and remyelination (1). Stem/progenitor cell transplantation of highly myelinogenic fetal or induced pluripotent stem cells-derived human oligodendrocyte progenitor cells (hOPCs) into the demyelinating disease remains an attractive means to achieve therapeutic remyelination (2). While substantial advances have been made in the preparation of hOPCs capable of mediating widespread myelination (3–5), poor survival of donor cells and maintenance of OPC fate are major barriers to the successful translation of this approach to clinical treatment. Current cell injection approaches are associated with substantial cell death with viability as low as 1 to 32% posttransplantation (6, 7), primarily due to cell membrane damage from shear stress (8–11). As a result, about 20% of transplanted cells survive after 1 week, and only 5% of cells remain viable 1-month postinjection (8). Some speculated that the extensional flow that is generated as cells move from the syringe to the much smaller diameter needle results in substantial deformation and stretching of cells, reducing cell viability (12, 13).

Extensive cell death exacerbates local inflammation, increasing the likelihood of graft failure (14).

Driven by the above considerations, shear-thinning hydrogels (STHs) have emerged as promising candidates for injection of Schwann cells, oligodendrocytes, or their stem cell precursors with minimal death. Injectable hydrogels with shear-thinning properties flow under shear stress and exhibit time-dependent recovery upon stress removal (15). Design of such hydrogels is based on the formation of dynamic physical bonds such as host-guest complexation (16–18), hydrogen bonding (19, 20), ionic interaction (21), polymer-nanocomposite interactions (22), and hydrophobic associations (23, 24) within the hydrogel network. Such noncovalent reversible interactions break upon application of force and reform upon relaxation, endowing the hydrogels with self-healing capacity and the ability to recover their storage modulus after application of shear stress (25).

Here, we report the development of innovative STHs with tunable bioactivity and viscoelastic properties to enhance the survival of transplanted hOPCs into a mouse model of hypomyelinating disease. Specifically, we used the *shiverer/rag2* mouse that models congenital hypomyelinating disease in humans such as Pelizaeus-Merzbacher disease and has become the gold standard for the assessment of myelinating cell preparations (5, 26–28). The results showed that the use of STH led to significantly higher cell viability posttransplantation, supported differentiation to myelin-forming oligodendrocytes, and increased myelination, demonstrating the potential of STH as an effective vehicle for hOPC delivery for treatment of myelin disorders.

## RESULTS

### Synthesis and characterization of supramolecular STHs

The building units used in the development of STHs are hyaluronic acid-thiol (HA-SH), heparin-thiol (Hep-SH), beta-cyclodextrin maleimide ( $\beta$ CD-Mal), and 8-arm polyethylene glycol adamantane (PEG-Ad) (Fig. 1). The development of STHs involves two key steps.

<sup>1</sup>Department of Chemical and Biological Engineering, University at Buffalo, The State University of New York (SUNY), Buffalo, NY, USA. <sup>2</sup>Department of Pharmacology and Toxicology, Jacobs School of Medicine and Biomedical Sciences, University at Buffalo, SUNY, Buffalo, NY, USA. <sup>3</sup>Neuroscience Program, Jacobs School of Medicine and Biomedical Sciences, University at Buffalo, SUNY, Buffalo, NY, USA. <sup>4</sup>Department of Biomedical Engineering, University at Buffalo, SUNY, Buffalo, NY, USA. <sup>5</sup>Center of Excellence in Bioinformatics and Life Sciences, University at Buffalo, SUNY, Buffalo, NY, USA. <sup>6</sup>Center of Cell, Gene and Tissue Engineering, University at Buffalo, SUNY, Buffalo, NY, USA.

\*Corresponding author. Email: fjsim@buffalo.edu (F.J.S.); sandread@buffalo.edu (S.T.A.)

†These authors contributed equally to this work.

‡Present address: Department of Chemistry, Faculty of Science, Mansoura University, Mansoura, 35516, Egypt.

§Present address: BioFrontiers Institute, University of Colorado–Boulder, 3415 Colorado Avenue, Boulder, CO 80303, USA.

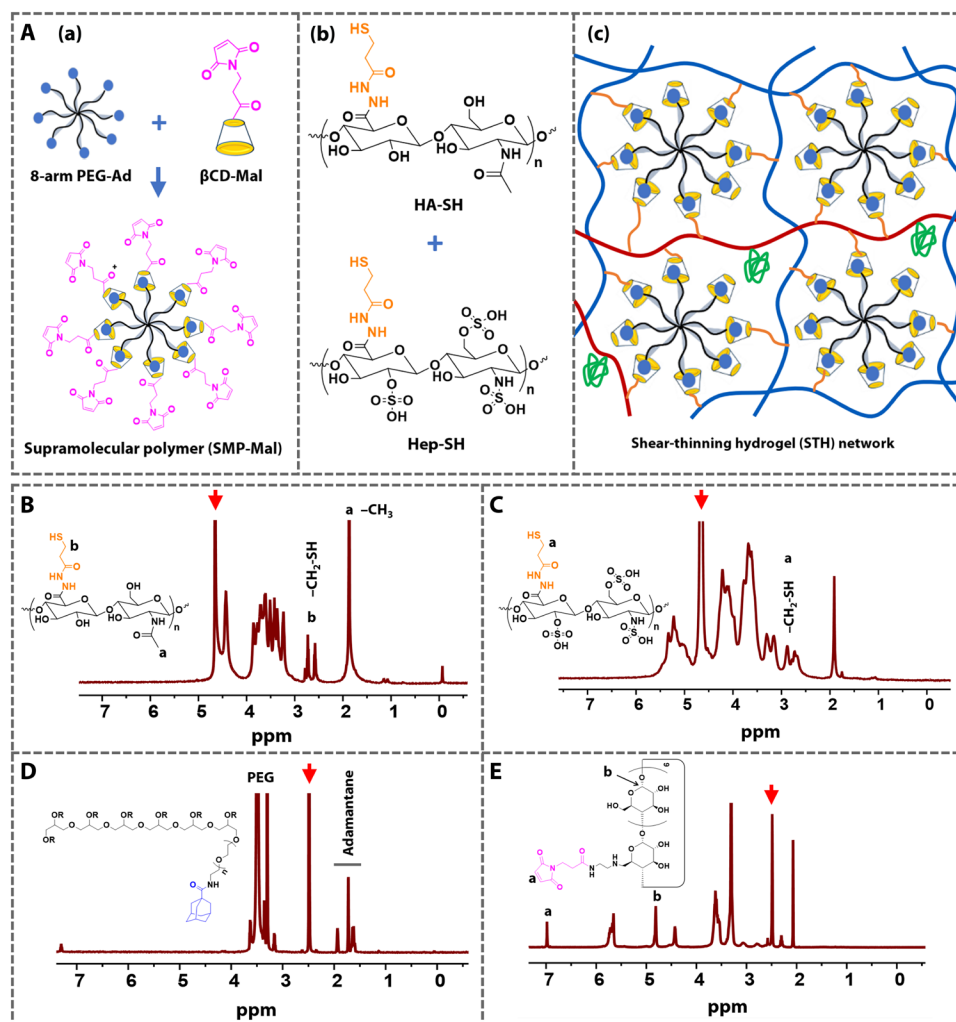


**Fig. 1. Schematic representation of the design of STHs and  $^1\text{H}$  NMR characterization of the hydrogel precursors.** (A) (a) Component 1 is the multiarm SMP incorporating maleimide terminals (SMP-Mal). It was developed by host-guest complexation between 8-arm PEG-Ad and monosubstituted  $\beta\text{CD}$ -Mal at 1:1  $\beta\text{CD}/\text{Ad}$  stoichiometric ratio. (b) Component 2 is the mixture of HA-SH and Hep-SH. (c) STH was formed by reacting SMP-Mal with a mixture of HA-SH (blue chain) and Hep-SH (red chain). The green color drawing represents biological cues. (B to E)  $^1\text{H}$  NMR analysis of (B) HA-SH ( $\text{D}_2\text{O}$  solvent), (C) Hep-SH ( $\text{D}_2\text{O}$  solvent), (D) 8-arm PEG-Ad ( $\text{DMSO}-d_6$ ), and (E)  $\beta\text{CD}$ -Mal ( $\text{DMSO}-d_6$ ). Red arrows represent the solvent signals.

The first step is the engineering of multiarm maleimide-terminated supramolecular polymer (SMP-Mal) through host-guest complexation between 8-arm PEG-Ad and mono-functionalized  $\beta\text{CD}$ -Mal at 1:1  $\beta\text{CD}/\text{Ad}$  stoichiometric ratio. The second step relies on Michael addition reaction between the 8-arm SMP-Mal and HA-SH at pH 7.4 to form the three-dimensional (3D) network. For immobilization of the pro-survival cues, Hep-SH was premixed with heparin-binding bidomain peptides and/or platelet-derived growth factor (PDGF)-AA and added to HA-SH before cross-linking with SMP-Mal.

HA-SH was developed by *N*-(3-dimethylaminopropyl)-*N'*-ethylcarbodiimide hydrochloride (EDC) coupling reaction between 3,3'-dithiobis(propanoic dihydrazide) (DTPDH) and the COOH groups of HA polymer, followed by redox cleavage of the disulfide bonds using tris-(2-carboxyethyl) phosphine (TCEP) (fig. S1A).  $^1\text{H}$  nuclear magnetic resonance (NMR) analysis of HA-SH revealed all signals from the corresponding chemical structure

and the characteristic  $\text{CH}_2\text{SH}$  signals appearing at 2.78 parts per million (ppm) (Fig. 1B). The degree of functionalization was 21.2% as calculated from the integration ratio of  $\text{CH}_3$  protons of HA at 1.89 ppm and the  $\text{CH}_2\text{SH}$  protons at 2.78 ppm. Similarly, Hep-SH was synthesized to enable the immobilization of the heparin-binding bioactive cues (fig. S1B).  $^1\text{H}$  NMR analysis confirmed the chemical structure and characteristic  $\text{CH}_2\text{SH}$  and  $\text{CH}_2\text{CH}_2\text{SH}$  signals appeared at 2.78 and 2.88 ppm, respectively (Fig. 1C). The thiol content of 0.25 mmol/g was calculated from the resonance intensity of  $\text{CH}_2\text{SH}$  protons at 2.78 ppm to that of the maleic acid internal standard at 6.31 ppm (fig. S2A). The 8-arm PEG-Ad was synthesized by the reaction of amine-terminated 8-arm PEG with adamantane-1-carboxylic acid in the presence of hexafluorophosphate azabenzotriazole tetramethyl uronium (HATU) coupling agent and diisopropylethylamine base (fig. S3A).  $^1\text{H}$  NMR analysis showed the distinct adamantane signals between 1.50 and 2.07 ppm, while the characteristic resonance of methylene protons

from PEG appeared between 3.22 and 3.81 ppm (Fig. 1D). It is worth noting that the  $CH_2NH_2$  protons of 8-arm PEG- $NH_2$  shifted from 2.83 to 3.19 ppm after the reaction, indicating quantitative conversion of the amine groups.  $\beta$ CD-Mal was synthesized by the reaction of mono(6-ethanediamine-6-deoxy)- $\beta$ -cyclodextrin ( $\beta$ CD- $NH_2$ ) and 3-maleimido-propionic NHS (*N*-hydroxysuccinimide) ester for 3 hours (fig. S3B). The chemical structure was confirmed by  $^1H$  NMR, and the ratio between the resonance intensity of the maleimide at 6.98 ppm (peak a) and C1 protons from cyclodextrin at 4.81 ppm (peak b) was 2:7, indicating mono-functionalization of the  $\beta$ CD ring (Fig. 1E). This result was corroborated by electrospray ionization mass analysis which revealed the agreement between the theoretical molecular mass (1328.46 Da) and the observed molecular mass (1329.19 Da) (fig. S4). Afterward, SMP-Mal was developed via host-guest complexation between 8-arm PEG-Ad and  $\beta$ CD-Mal at 1:1  $\beta$ CD/Ad molar ratio (fig. S3C). The host-guest interaction between the 8-arm PEG-Ad and  $\beta$ CD-Mal was confirmed by two-dimensional rotating frame Overhauser effect spectroscopy (2D ROESY) NMR using deuterium oxide ( $D_2O$ ) solvent (fig. S2B).

Next, STHs were developed by reacting a mixture of HA-SH and Hep-SH with SMP-Mal at pH 7.4 via Michael addition reaction (Fig. 1A, a to c). The hydrogels were prepared by varying the amounts of each of the two components, HA-SH and SMP-Mal. Specifically, the compositions were STH-1 (HA<sub>2wt%</sub>SMP<sub>3.3wt%</sub>, stiff), STH-2 (HA<sub>1.3wt%</sub>SMP<sub>6.6wt%</sub>, intermediate stiffness), and STH-3 (HA<sub>0.66wt%</sub>SMP<sub>10wt%</sub>, soft) (table S1). Supramolecular hydrogels

incorporating host-guest dynamic bonds exhibit shear-thinning and self-healing characteristics due to the dynamic reversibility of the  $\beta$ CD-Ad complexation under shear stress (Fig. 2A), making them suitable for injection of therapeutics. STHs were formed immediately ( $\sim 10$  s) after mixing HA-SH/Hep-SH and multiarm SMP-Mal due to the fast reaction kinetics of thiol-maleimide addition. As a result, it was difficult to measure the gelation time by time sweep rheology. Instead, the gelation time was assessed by the tube inversion method, i.e., by measuring the time required for the liquid macromers to transition into a nonflowing state (fig. S5, A to C). For STH-1 and STH-2, the time was 9 and 15 s, respectively, while the time could not be precisely determined for STH-3 because it is very soft, exhibiting liquid-like behavior. Unlike STH-3, free-standing STH-1 and STH-2 were able to withstand their weight and maintain a 3D structure after 24 hours, as indicated by qualitative assessment using the tilted tube method (fig. S5D).

Rheological measurements were performed to reveal the mechanical and rheological properties of the STHs. An oscillatory frequency sweep test at 0.5% strain showed a frequency-dependent increase of storage modulus ( $G'$ ) and loss modulus ( $G''$ ) of the STHs, which is characteristic of viscoelastic networks formed by the assembly of host-guest bonds (Fig. 2B and fig. S6, A to C). STH-1 and STH-2 showed higher  $G'$  than  $G''$ , indicating elastic-like behavior, while for STH-3,  $G''$  surpassed  $G'$ , revealing a viscous-like behavior due to the excess SMP-Mal over the thiol groups (Fig. 2, B to D). At 10 rad/s, the storage modulus increased in the order of

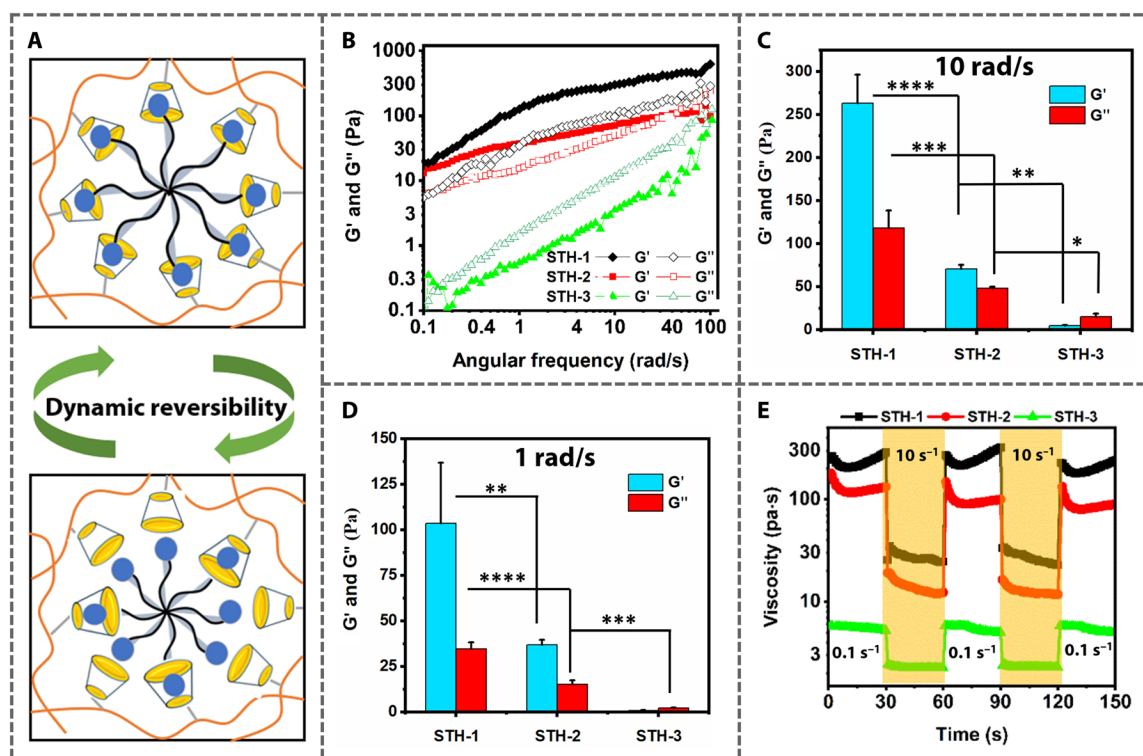


**Fig. 2. Viscoelasticity and rheological properties of STHs.** (A) Dynamic reversibility of STH network. (B) Storage modulus ( $G'$ ) and loss modulus ( $G''$ ) of STH-1, STH-2, and STH-3 at oscillatory frequency. (C and D)  $G'$  and  $G''$  of STH-1, STH-2, and STH-3 at a frequency of (C) 10 rad/s and (D) 1 rad/s. (E) Shear-thinning and self-healing of STHs at cyclic shear rates of 0.1 and 10.0  $s^{-1}$ . Data are mean  $\pm$  SD. \* $P < 0.05$ , \*\* $P < 0.005$ , \*\*\* $P < 0.0005$ , and \*\*\*\* $P < 0.0001$ , one-way analysis of variance (ANOVA) with Tukey's post hoc test.  $n = 3$  to 4 STH samples.

STH-1 > STH-2 > STH-3, reaching ~263, 70, and 4 Pa, respectively (Fig. 2B).

Next, we assessed the shear-thinning property and recovery timescale of the hydrogels by monitoring the viscosity at high ( $10.0 \text{ s}^{-1}$ ) and low ( $0.1 \text{ s}^{-1}$ ) shear rates (Fig. 2E and fig. S6, D to F). At high shear rate, STHs showed a sharp decrease in viscosity, indicating disassembly of the host-guest bonds and more fluid-like behavior. At a low shear rate, the hydrogels recovered the initial viscosity within seconds, indicating self-healing due to the rapid assembly of the host-guest bonds (Fig. 2E). The fast transition from solid-like to fluid-like behavior with increasing shear rate is essential for successful injection and cell protection, as it enables energy dissipation by the flowing hydrogel during injection and recovery of the storage modulus after injection to stabilize the material at the injection site.

Last, the stress-relaxation rate of STHs was assessed by measuring the stress-relaxation half-time ( $t_{1/2}$ , the time required for the stress to reach half of its initial value) under constant 10% strain. All STH networks showed fast relaxation time ( $t_{1/2} < 1 \text{ s}$ ), indicating the fast dynamics of the host-guest networks; with  $t_{1/2}$  of each hydrogel in the order STH-1 > STH-2 > STH-3 (fig. S7, A and B).

### In vitro degradation of the STHs

Degradability and matrix remodeling of hydrogel scaffolds are crucial for directing cell behavior. We assessed the degradation of STHs by hydrolysis in phosphate-buffered saline (PBS) at  $37^\circ\text{C}$ , and the degradation profile was studied by spectrophotometric monitoring of the HA byproducts. To this end, the HA released from STH was treated with the enzyme hyaluronidase that breaks the  $\beta(1,4)$ -glycosidic bond of the HA disaccharide unit (Fig. 1A, b) (29, 30), yielding glucuronic acid and *N*-acetyl-D-glucosamine (NAG), which was measured using Ehrlich's reagent (fig. S8). The time it takes for NAG to reach 50% of the total is the half-life of degradation, which was measured to be  $8.18 \pm 0.07\%$ ,  $8.12 \pm 0.80\%$ , and  $6.38 \pm 0.16\%$  for STH-1, -2, and -3, respectively (fig. S8).

### Enhanced OPC viability with STH under shear stress in vitro

One of the major barriers to successful cell transplantation for the treatment of neurodegenerative diseases is the low survival of donor cells when delivered by minimally invasive injection. More than 95% of neural progenitor cells (NPCs) transplanted into models of spinal cord injury (SCI) die following injection (31, 32), most likely via shear stress on the cell membrane (8). We hypothesized that STH may reduce cell death under shear and improve cell delivery to treat demyelinating diseases.

To this end, we measured cell death after passage through a pulled glass needle [internal diameter (ID): 100 to 200  $\mu\text{m}$  equivalent to 28- to 32-G needle] in the absence or presence of STH at an injection rate of 0.1  $\mu\text{l}$  every 5 s. Using a live-dead assay, we found that rat oligodendrocyte progenitors (CG-4 cell line) and human fetal CD140a-sorted primary oligodendrocyte progenitor cells (hOPC) exhibited  $29.47 \pm 3.15\%$  (fig. S9) and  $25.13 \pm 3.23\%$  (Fig. 3) cell death, respectively, when injected in saline solution [Hanks' balanced salt solution (HBSS)], as compared to only  $6.63 \pm 1.60\%$  (CG-4) and  $6.57 \pm 0.71\%$  (hOPC), respectively, in the absence of shear stress [no shear (NS)]. All three STH formulations reduced cell death of both CG-4 and hOPC significantly as compared to saline control (CG-4: STH-1:  $21.30 \pm 0.46\%$ ,  $P = 0.0008$ ; STH-2:  $11.23 \pm 1.44\%$ ,  $P < 0.0001$ ; STH-3:  $13.50 \pm 1.18$ ;  $P < 0.0001$ ,

Dunnett's post hoc test) (hOPC: STH-1:  $16.30 \pm 3.05\%$ ,  $P = 0.0038$ ; STH-2:  $10.63 \pm 2.10\%$ ,  $P < 0.0001$ ; STH-3:  $13.83 \pm 2.03\%$ ;  $P = 0.0006$ , Dunnett's post hoc test). Minimal or insignificant differences (CG-4:  $P = 0.0337$ ; hOPC:  $P = 0.1834$ , Dunnett's post hoc test) were observed between the STH-2 formulation and the NS group. Therefore, STH-2 provided the highest level of protection from cell death under injection-shear.

### Evaluation of biological cues to promote hOPC survival

We hypothesized that an immobilization of biological cues in STH might further promote their survival and proliferation after transplantation. Both precursor and mature oligodendrocytes highly express  $\alpha_v/\alpha_6/\alpha_7$  and  $\beta_1/\beta_5/\beta_8$  integrins, guiding their survival, proliferation, and terminal differentiation to myelinate the neuronal axons (33, 34). Using RNA sequencing (RNA-seq), we also determined the expression of various integrins in hOPCs using two fetal replicates cultured at high and low density (table S2). The hOPCs showed high expression of several alpha [ $\alpha_v = 82.6 \pm 2.19$ ,  $\alpha_7 = 47.1 \pm 3.15$ ; fragments per kilobase of transcript per million mapped reads (FPKM)] and beta ( $\beta_1 = 116.8 \pm 1.45$ ,  $\beta_8 = 126.2 \pm 8.34$  FPKM) integrin subunits. Therefore, as shown in fig. S10 (A and B), we designed an innovative bidomain peptide, heparin-binding domain (HBD)-RGD5 to promote cell binding via integrins  $\alpha_5\beta_1$ ,  $\alpha_v\beta_1$ , or  $\alpha_v\beta_8$  (35–38). A second bidomain peptide, HBD-REDV5, was used as negative control, as these cells express very low levels of  $\alpha_4$  integrin (FPKM =  $0.8 \pm 0.3$ , as shown in the RNA-seq data; table S2). The fusion peptides consist of two domains: (i) the HBD2 of fibronectin that enables immobilization into the hydrogel by binding to Hep-SH and (ii) five tandem repeats of (GGGS-HIPREDVDYH) or (GGGS-GRGDS) that bind to cells (fig. S10, A and B).

First, we evaluated the bidomain fusion proteins, which were immobilized onto poly-D-lysine (PDL)-bound heparin via their HBD (fig. S10B). Following overnight incubation of the heparin-coated surfaces with the bidomain peptides, rat CG-4 cells were seeded for 48 hours. Quantification of cell area indicated significant cell attachment and spreading on HBD-RGD5 compared to control (PDL alone) but not on HBD-REDV5, where cells appeared mostly round with reduced mean cell area (fig. S10, C to F). Next, we examined the binding of hOPCs on various concentrations of heparin-immobilized HBD-RGD5 (Fig. 4, A and H). The average number of cells per field (Fig. 4B) and the proportion of EdU<sup>+</sup> cells (Fig. 4C) increased with increasing concentration of HBD-RGD5 compared to the control on laminin (Lam)-coated surface (Fig. 4G), indicating increased hOPC proliferation.

PDGF-AA promotes hOPC survival and proliferation via platelet-derived growth factor receptor  $\alpha$ , which is highly expressed on their surface and decreases as they differentiate toward mature oligodendrocytes (4). Therefore, we examined the dose dependence of PDGF-AA on human primary CD140a/PDGFR<sup>+</sup> OPC proliferation in vitro (Fig. 4, D and I). To this end, the cells were starved for 24 hours and then cultured with the indicated concentrations of PDGF-AA (0.5 to 200 ng/ml) for the next 24 hours. PDGF-AA increased the proliferation of hOPCs in a dose-dependent manner as shown by increased cell number per square millimeter (Fig. 4E) and percentage of EdU<sup>+</sup> cells (Fig. 4F). The highest proliferation rate was achieved with PDGF-AA (100 ng/ml; ~40% EdU<sup>+</sup>) beyond which proliferation reached a plateau.

We also assessed the potential of hOPC differentiation on HBD-RGD5 by immunostaining for immature oligodendrocyte marker,

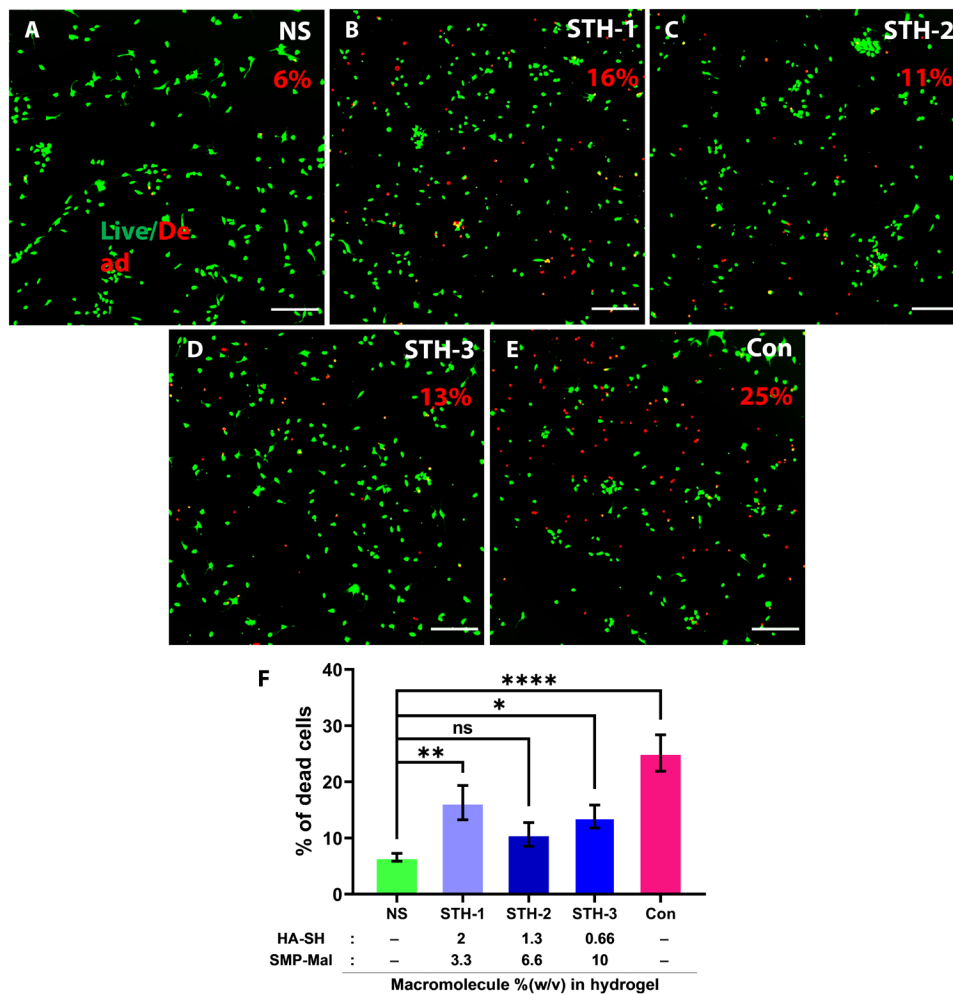


**Fig. 3. In vitro evaluation of hOPC survival after injection with STHs.** (A to E) Representative images of hOPCs after passing through a pulled glass needle (ID = 100 to 200  $\mu\text{m}$ ) in the presence of the indicated STH preparations. Con: Control cells were passed through the needle in HBSS, and NS: cells plated without passing through the needle (NS). Scale bars, 200  $\mu\text{m}$ . (F) Quantification of the percentage of dead cells evaluated at 3 hours postseeding using the Live-Dead assay (calcein-ethidium homodimer). Data are presented as mean  $\pm$  SD. not significant (ns)  $P \geq 0.05$ , \* $P < 0.05$ , \*\* $P < 0.005$ , \*\*\*\* $P < 0.0001$ , one-way ANOVA with Dunnett's post hoc test.  $n = 3$  independent experiments.

O4, at 4 days after mitogen removal (Fig. 5, A to F). Upon removal of PDGF-AA, hOPCs exited the cell cycle and adopted a relatively mature oligodendrocyte phenotype within 4 days, which was evident by the appearance of the complex network of branched processes both on control and HBD-RGD5 substrates (Fig. 5, A to F). The hOPC cell number increased gradually with increasing concentration of HBD-RGD5, even in the absence of PDGF-AA and neurotrophin-3 (NT-3) in the culture medium (Fig. 5G). The percentage of O4<sup>+</sup> hOPCs remained constant at 20% up to 12.5 nmol/cm<sup>2</sup> and gradually declined at higher HBD-RGD5 concentrations (Fig. 5H). The percentage of O4<sup>+</sup> hOPCs on bidomain fusion peptide at 50 nmol/cm<sup>2</sup> concentration was significantly lower ( $P < 0.05$ ) than the control surface (Lam) and HBD-RGD5 concentrations of 12.5 nmol/cm<sup>2</sup> or lower, suggesting that, at high concentrations, the peptide inhibited differentiation. Therefore, we used the HBD-RGD5 fusion peptide at 12.5 nmol/cm<sup>2</sup> for all future experiments.

### Survival, differentiation, and migration of the hOPCs within the STH

Here, we assessed the survival of hOPCs within a 3D hydrogel environment in vitro using three different STH formulations. All three hydrogels supported survival of hOPCs to a similar extent (cell death: STH-1:  $7.10 \pm 1.03\%$ , STH-2:  $5.97 \pm 2.19\%$ , STH-3:  $5.58 \pm 0.97\%$ ;  $P > 0.05$ , Tukey's post hoc test) as shown in fig. S11, with no significant differences when compared to cells cultured on 2D Lam (Fig. 3; NS:  $6.57 \pm 0.7\%$ ,  $P > 0.05$ , Tukey's post hoc test). Despite similarities in overall survival (fig. S11), the distribution of cells was different among the three hydrogels. Specifically, STH-1 and STH-3 contained cell clusters (STH-1: 13 to 16 clusters/mm<sup>2</sup>; STH-2: 9 to 12 clusters/mm<sup>2</sup>,  $n = 3$ ), whereas in STH-2, the cells were distributed more uniformly (STH-3: four to six clusters/mm<sup>2</sup>,  $n = 3$ ). This observation might be attributed to the limited cell migration in STH-1 (stiff, 263 Pa) and insufficient mechanical support in STH-3 (soft, 4 Pa).

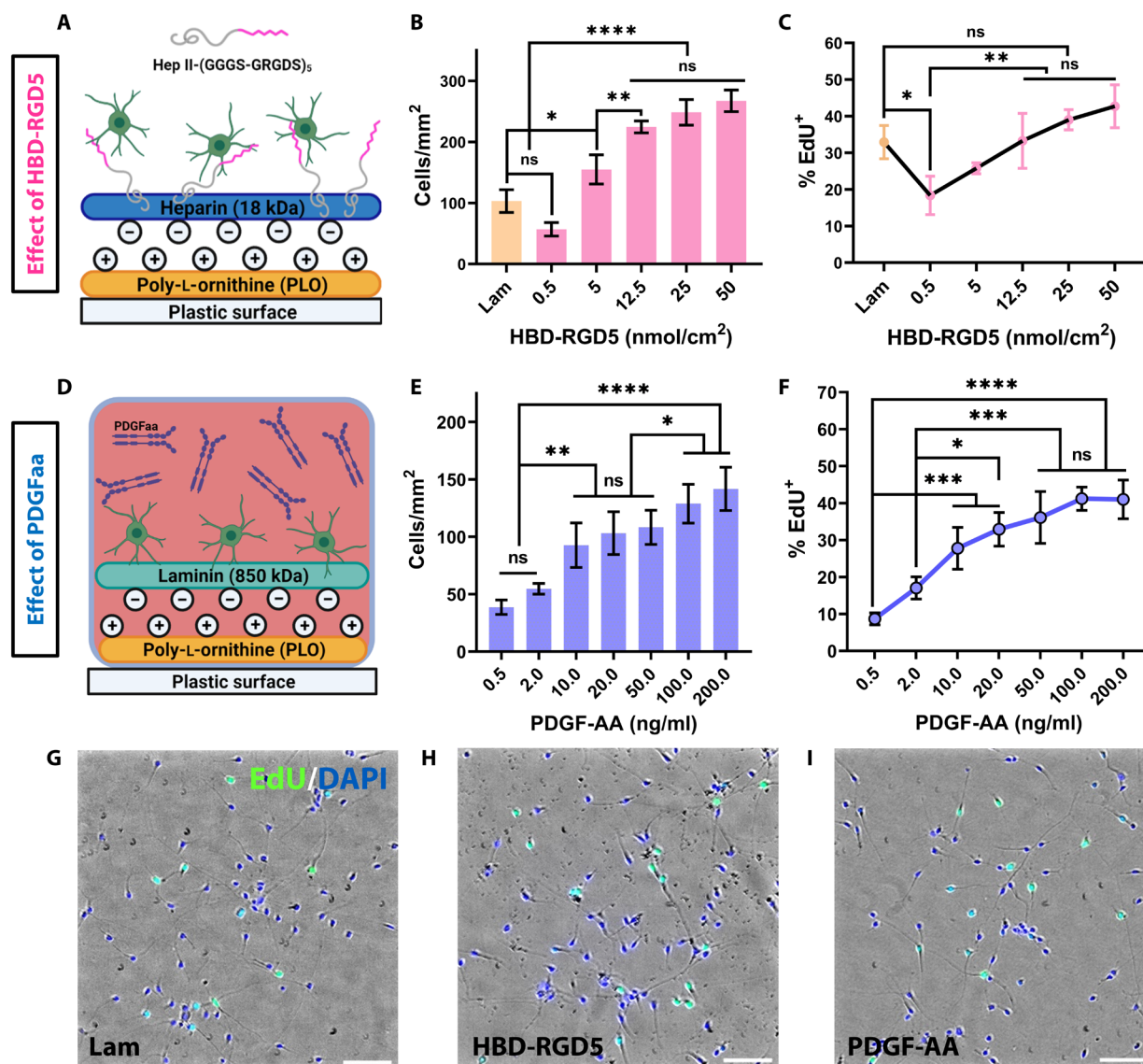


**Fig. 4. Proliferation of the hOPCs in response to biological cues.** (A and D) Schematic of the experimental setup to evaluate the mitogenic response of hOPCs to HBD-RGD5 peptide or PDGF-AA. The cells were cultured for 48 hours either on (A) wells with the indicated concentrations of immobilized HBD-RGD5 peptide or (D) Lam-coated wells in the presence of the indicated concentrations of PDGF-AA. (B and E) Quantification of the number of hOPCs per square millimeter as a measure of cell growth in response to the (B) HBD-RGD5 peptide or (E) PDGF-AA, respectively. (C and F) Quantification of the hOPC proliferation as percentage of EdU<sup>+</sup> cells in response to the biological cues. EdU was detected by labelling with a fluorescently tagged azide via a specific click reaction as per manufacturer's protocol. (G to I) Representative images of the hOPCs on (G) control/Lam surface, (H) HBD-RGD5 (12.5 nmol/cm<sup>2</sup>), or (I) PDGF-AA (100 ng/ml). Scale bars, 200  $\mu$ m. Data are mean  $\pm$  SD. ns,  $P \geq 0.05$ ; \* $P < 0.05$ ; \*\* $P < 0.005$ ; \*\*\* $P < 0.0005$ ; and \*\*\*\* $P < 0.0001$ ; one-way ANOVA with Tukey's post hoc test.  $n = 3$  independent experiments with three different donors.

Next, we investigated hOPC differentiation within each hydrogel in 3D, in the absence of mitogens for 4 days. Intermediate (STH-2) and low stiffness (STH-3) hydrogels supported hOPC differentiation, but the stiffer formulation (STH-1) did not (STH-1:  $2.23 \pm 0.86\%$ ; STH-2:  $13.63 \pm 1.15\%$ ; STH-3:  $17.30 \pm 0.78\%$  O4<sup>+</sup> cells). As expected, the percentage of O4<sup>+</sup> OPCs was significantly lower than the cells differentiated on Lam-coated tissue culture plastic ( $23.24\% \pm 1.98\%$ , STH-2:  $P = 0.0019$ , STH-3:  $P = 0.0085$ ; two-tailed unpaired  $t$  test). In addition, O4<sup>+</sup> hOPCs within the hydrogels exhibited a round morphology with small number of processes indicative of immature oligodendrocytes

(fig. S12), in contrast to cells on tissue culture plastic that exhibited a complex network of branched processes upon differentiation (Fig. 5 and fig. S12A). These results are in agreement with previous observations, where OPC differentiation was hindered in stiff as compared to soft hydrogels (39, 40), indicating that there may be an optimal hydrogel stiffness promoting OPC differentiation in 3D.

Together, STH-2 demonstrated the highest level of protection for the CG-4 cells (fig. S9) and hOPCs (Fig. 3) against injection-induced shear stress. In addition, STH-2 maintained a more uniform cell distribution (fig. S11) and supported oligodendroglial differentiation

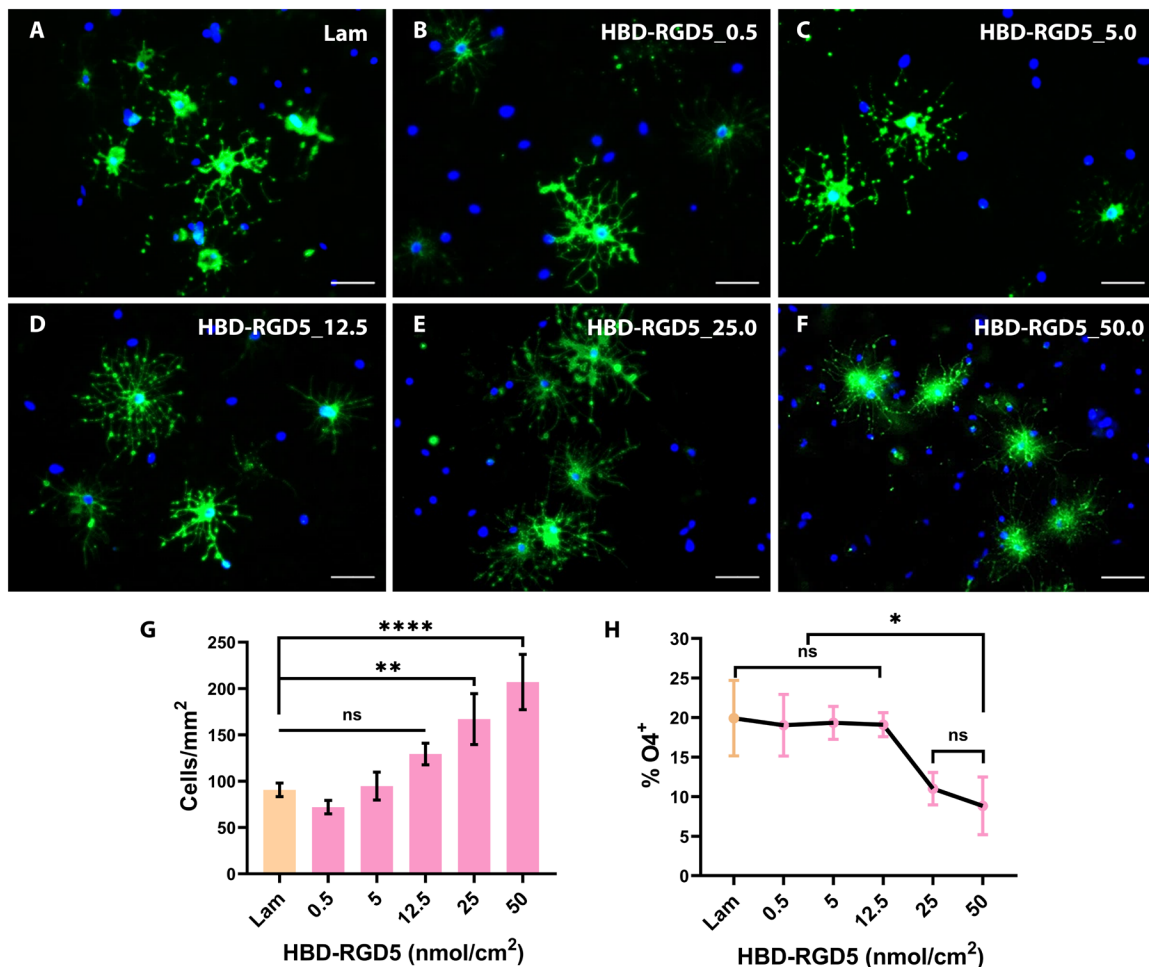


**Fig. 5. Differentiation of the hOPCs on bidomain fusion peptide, HBD-RGD5.** The *in vitro* differentiation potential of the hOPCs toward oligodendrocyte fate was evaluated by staining for the oligodendrocyte marker, O4. The cells were cultured on the indicated concentrations of surface immobilized HBD-RGD5 for 4 days in GF-free ND media. (A to F) Representative immunofluorescence images for O4 expression on control/Lam and surfaces with HBD-RGD5 peptide immobilized at the indicated concentrations. Scale bars, 50  $\mu$ m. (G) Quantification of the number of hOPCs per square millimeter on Lam and HBD-RGD5 immobilized surfaces at the indicated concentrations. (H) Quantification of the percentage of O4<sup>+</sup> cells as a function of peptide surface concentration. Data are mean  $\pm$  SD. ns,  $P \geq 0.05$ ; \* $P < 0.05$ ; \*\* $P < 0.005$ ; and \*\*\*\* $P < 0.0001$ ; one-way ANOVA with Tukey's post hoc test.  $n = 3$  independent experiments with three different donors.

(fig. S12). For these reasons, STH-2 was selected for all subsequent *in vitro* and *in vivo* studies.

Given the need for transplanted hOPCs to migrate a considerable distance from the injection site after transplantation, we also investigated cell binding and migration within the STH-2 *in vitro*. To this end, STH-2 conjugated with various concentrations of HBD-RGD5 was placed on top of a transwell membrane (fig. S13A), and cells were introduced on top of the hydrogel in basal media. At the same time, PDGF-AA (100 ng/ml) was added in the lower chamber to generate a chemotactic gradient. The cells migrated through the hydrogel to the other side of the transwell membrane, but the number of migrating cells decreased with increasing concentrations of immobilized HBD-RGD5 (fig. S13B), indicating increased cell binding within the hydrogel in 3D. Movie S1 demonstrates a visual depiction of cell migration within the hydrogel over a 16-hour period. Images of multiple planes (z-stack, 1-mm thick) were merged to create the video, showcasing the movement of the cells from the top to the bottom of the hydrogel.

### Enhanced hOPC survival *in vivo* via STH-assisted transplantation

An immunodeficient NSG mouse (NOD scid gamma mouse, lacking mature T, B, and natural killer cells) was used to evaluate hOPC survival after transplantation *in vivo*. As shown in Fig. 6A, hOPCs were injected unilaterally into the 2- to 3-day-old mouse brain following cryoanesthetization. Each animal received 0.5  $\mu$ l of cells (100,000 cells/ $\mu$ l) either in HBSS, STH-2 alone, or STH-2 with PDGF-AA and HBD-RGD5 using a Hamilton syringe equipped with a pulled glass needle (ID = 100 to 200  $\mu$ m). Pups were euthanized at 6 weeks post-implantation, and the brains were isolated according to the approved Institutional Animal Care and Use Committee protocol. Brain sections were analyzed at 0.16-mm intervals by staining with human nuclear antigen (hNA). As control, we injected Cy5.5-conjugated STH-2 without cells and observed that the hydrogel stayed at the injection site within the corpus callosum (CC) region of the brain during the 14-day observation window (fig. S14).

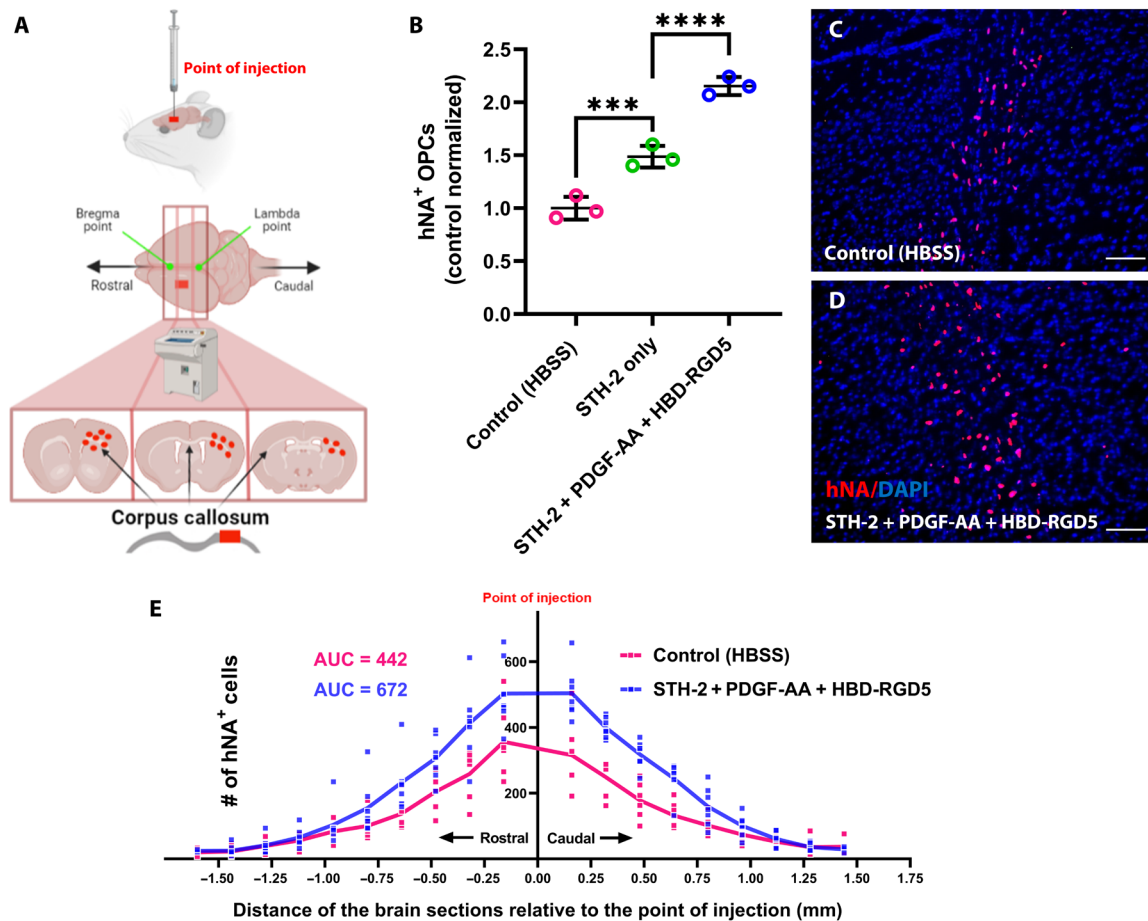


**Fig. 6. Increased survival of the hOPCs in the NSG mouse brain upon transplantation with STH-2 and immobilized biological cues.** (A) Schematic of the animal transplantation protocol. CD140a<sup>+</sup> hOPCs were injected unilaterally into the left hemisphere of the immunocompromised, NSG mice at 100,000/μl within 2 to 3 days of birth. The animals were euthanized at 6 weeks postinjection, and brain sections of 16-μm thickness were collected from rostral to caudal direction throughout the fore-brain. The red rectangle indicates the site/point of injection, and the red dots present the transplanted human cells. (B) Number of transplanted hNA<sup>+</sup> OPCs in HBSS, STH-2 alone, or STH-2 plus PDGF-AA and HBD-RGD5. Data are mean ± SD. \*\*\**P* < 0.0005 and \*\*\*\**P* < 0.0001, one-way ANOVA with Tukey's post hoc test. *n* = 3 animals per condition. (C and D) Representative images of the CC region of the brain sections receiving cells in HBSS or hydrogel. Scale bars, 100 μm. (E) Spatial distribution of hNA<sup>+</sup> OPCs injected into the brain CC with either HBSS (control) or STH-2 plus PDGF-AA and HBD-RGD5. Calculation of the area under each curve (AUC) demonstrated 52% higher cell survival in the hydrogel group as compared to control condition. Data are the hNA<sup>+</sup> cell count for each brain section per animal, *n* = 6 to 7 animals per condition, animals were from two different litters, and the transplanted hOPCs were also from with two different donors.

Consistent with our *in vitro* survival data (Fig. 3), animals receiving cells embedded in hydrogel showed significantly (*P* < 0.0001) higher number of hNA<sup>+</sup> hOPCs as compared to the control (HBSS) group (Fig. 6B). Immobilization of PDGF-AA and HBD-RGD5 (STH-2 + PDGF-AA + HBD-RGD5 group) further increased the number of hNA<sup>+</sup> cells (*P* < 0.0001) in the mouse brain compared to STH-2 alone.

The spatial distribution of hNA<sup>+</sup> cells showed that the injected cells dispersed and migrated almost 1500 μm in the anterior/posterior axis from the point of injection, suggesting a migration rate of approximately >30 μm/day. Calculation of the area under the curve indicated 52% higher survival of hOPCs delivered in the STH-2 with PDGF-AA and HBD-RGD5 as compared to the control (HBSS) group (Fig. 6E). However, the observed increase of hOPCs at 6 weeks postinjection with STH might also be attributed to increased proliferation due to the interaction with the STH and/or the biological cues rather than enhanced survival immediately after injection as modeled *in vitro*.

### Improved myelination of the shiverer mouse brain by STH delivery of hOPCs

We evaluated the myelination potential of STH-transplanted hOPC cells in a *shiverer/rag2* mouse, a model of congenital hypomyelinating disease that has become the gold standard for the assessment of myelinating cell preparations (5, 26–28). To this end, we injected hOPCs (0.5 μl at 100,000 cells/μl) bilaterally into the CC of neonatal (2- to 3-day-old) *shiverer/rag2* mice (*n* = 4 to 5 per condition) as described previously (4, 28). Cells were injected in HBSS or STH-2 with immobilized PDGF-AA and HBD-RGD5; the mice were euthanized 12 weeks later, and brain sections were immunostained for hNA to detect hOPCs. The site of implantation was determined as the site with maximal density of hNA<sup>+</sup> cells in coronal sections.

Immunostaining with myelin basic protein (MBP) identified widespread myelination that was primarily restricted to the CC (Fig. 7, A and B). Mature myelin was observed in both control and hydrogel groups across a region spanning approximately 650 ± 160 μm

along the rostrocaudal axis from the site of injection. Quantification of transplanted cell-mediated myelination via immunofluorescence for MBP indicated significant enhancement following delivery of hOPCs in STH compared to the HBSS control group (Fig. 7C). In the STH-2 + PDGF-AA + HBD-RGD5 group, we observed increased MBP<sup>+</sup> area toward the rostral (6 to 10%,  $P < 0.005$ ) and caudal (5 to 7%,  $P < 0.05$ ) directions from the point of injection.

Consistent with improved cell survival in STH, the total number of engrafted hNA<sup>+</sup> hOPCs was significantly higher when injected with STH-2-containing PDGF-AA and HBD-RGD5 (Fig. 7D;  $P < 0.005$ , one-tailed unpaired  $t$  test).

To determine whether STH-2 with PDGF-AA and HBD-RGD5 altered the pattern of differentiation of engrafted hOPCs, we assessed the fate of human hNA<sup>+</sup> cells (Fig. 7, E to H). The percentage of

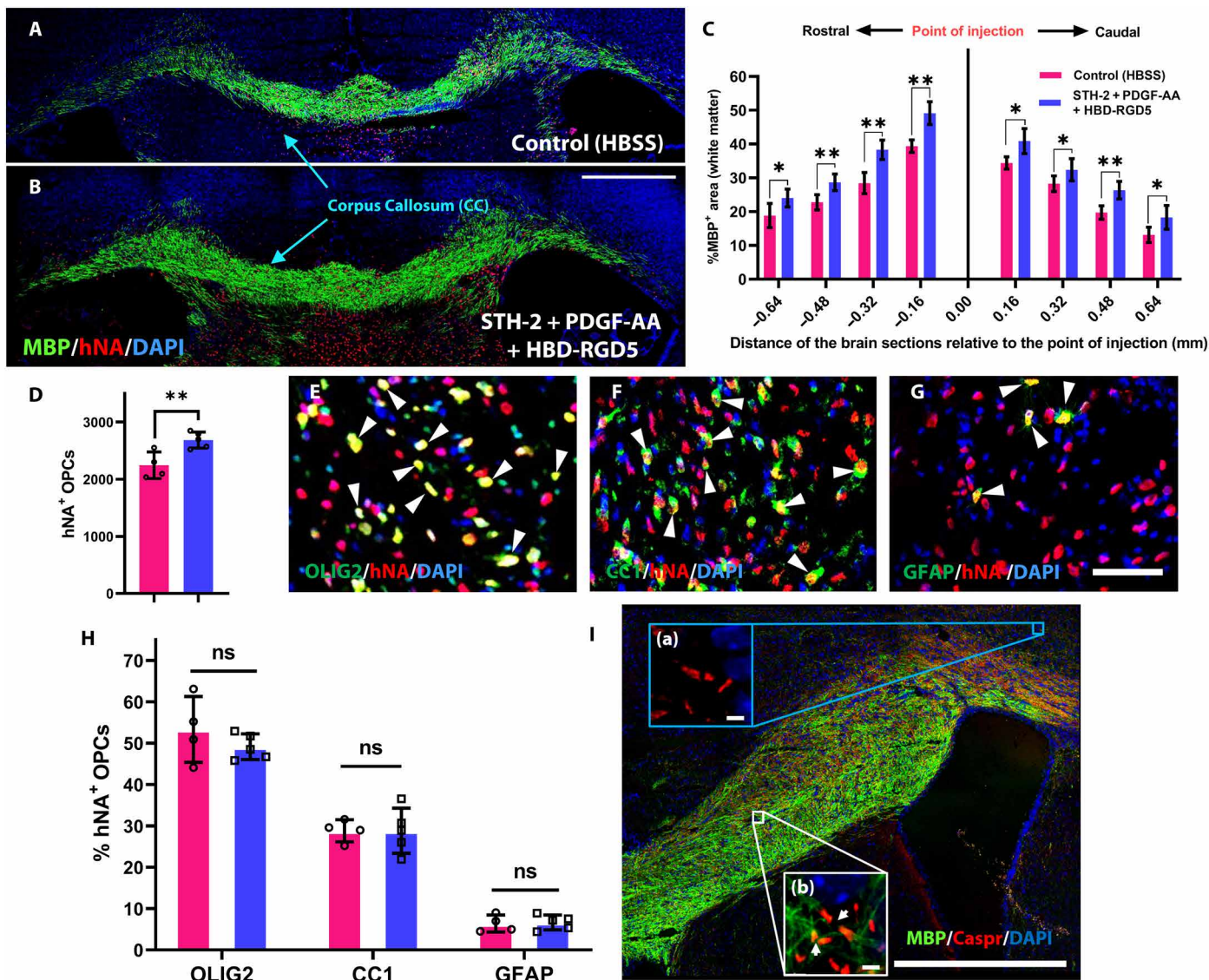


**Fig. 7. Increased myelination of the *shiverer/rag2* mouse brain upon delivery of the hOPCs with STH-2 fortified with biological signals.** (A and B) Representative confocal microscopy images of the hypomyelinating brain sections immunostained for MBP (green) and hNA (red) at 12 weeks posttransplantation. hOPCs were transplanted either in HBSS (control) or STH-2 + PDGF-AA + HBD-RGD5. (C) Quantification of the myelinated regions (MBP<sup>+</sup>) of the white matter shows a significant increase in myelination in the STH-2 plus biological cues group compared to the control. Data are mean ± SD. \* $P < 0.05$  and \*\* $P < 0.005$ , two-tailed unpaired  $t$  test for the respective brain sections, (D) Quantification of the number of hNA<sup>+</sup> OPCs with STH-2 + PDGF-AA + HBD-RGD5 compared to the control. Data are mean ± SD, \*\* $P < 0.005$ , one-tailed unpaired  $t$  test. (E to G) Representative sections of mouse brain transplanted with hOPCs in STH-2 + PDGF-AA + HBD-RGD5 stained for markers of oligodendrocytes (OLIG2), postmitotic oligodendrocytes (CC1), and astrocytes (GFAP). White arrowheads indicate staining colocalized with hNA. (H) Quantification of the OLIG2<sup>+</sup>, CC1<sup>+</sup>, and GFAP<sup>+</sup> cells as a percentage (%) of total hNA<sup>+</sup> hOPCs. Data are mean ± SD. ns,  $P \geq 0.05$ , two-tailed unpaired  $t$  test between the two groups. (I) Immunofluorescence images of *shiverer/rag2* mouse brain stained for MBP (green) and Caspr (red) at 12 weeks posttransplantation. (a) Unmyelinated regions of the brain lacking organized nodes of Ranvier. (b) Densely myelinated region of the CC containing organized nodes of Ranvier, in places where the axonal Caspr protein was in close apposition to human MBP<sup>+</sup> internodes. White arrows in (b) indicate normal nodes of Ranvier.  $n = 4-5$  animals per condition from three different litters; transplanted hOPCs were from with three different donors. Scale bars, 500  $\mu\text{m}$  [(A), (B), and (I)], 50  $\mu\text{m}$  [(D) to (F)], and 2.5  $\mu\text{m}$  (a and b).

oligodendrocytes (OLIG2<sup>+</sup>; Fig. 7, E and H) (STH-2 + PDGF-AA + HBD-RGD5: 49.12 ± 3.09%; control: 53.33 ± 7.96%,  $P > 0.05$ ) and postmitotic oligodendrocytes (CC1<sup>+</sup>; Fig. 7, F and H) (STH-2 + PDGF-AA + HBD-RGD5: 28.82 ± 5.45%; control: 27.82 ± 3.03%,  $P > 0.05$ , two-tailed unpaired *t* test) was similar in both groups. Likewise, the proportion of hOPCs undergoing astrocyte differentiation [glial fibrillary acidic protein–positive (GFAP<sup>+</sup>); Fig. 7, G and H] remained similar (STH-2 + PDGF-AA + HBD-RGD5: 6.65 ± 1.78%; control: 6.38 ± 2.06%,  $P > 0.05$ ). These results indicated that STH-2 + PDGF-AA + HBD-RGD5 did not alter the fate of hNA<sup>+</sup> cells. Rather, the principal effect of the fortified hydrogel was to increase cell viability postinjection, thereby accelerating the production of myelinating oligodendrocytes.

*Shiverer* brains lacking compact myelin display paranodal disruption and cannot form nodes of Ranvier (41), which are required for establishment of saltatory conduction in myelinated axons. As shown previously (26), in regions of dense hOPC engraftment and MBP expression, we observed restoration of nodal structures as demonstrated by paranodal expression of axonal Caspr protein in close apposition to MBP<sup>+</sup> internodes (Fig. 7I). These data are therefore consistent with myelin restoration in the transplanted animals. Therefore, we conclude that STH-assisted hOPC delivery provides an attractive approach to improve stem cell delivery for therapeutic myelination.

## DISCUSSION

Following transplantation in the brains of congenitally hypomyelinated and cuprizone-induced demyelinated mice, hOPCs tend to migrate into and along white matter tracts resulting in robust myelination of host axons (42, 43). The migratory phenotype and myelination potential render hOPCs a promising candidate for cell-based therapy to treat demyelinating diseases of the central nervous system (CNS) (43, 44). However, clinical translation is limited by major barriers, including poor survival of donor cells and maintenance of the OPC fate. Previous studies reported that only a small fraction (≤5%) of the injected cells, including human adipose-derived stem cells (45), cardio-myoblasts (46), mesenchymal stem cells (MSCs) (47), and NPCs (32), remain viable at 1 to 2 weeks after injection in saline or cell culture media. Specifically, only 1 to 3% of NPCs have been reported to survive after transplanting into ischemic brain tissue (48, 49). Schwann cells, the myelin-forming cells of the peripheral nervous system, also suffer from massive cell death (>95%) after transplantation due to high shear stress during injection causing cell membrane rupture (8). Although the hOPCs can survive and proliferate post-implantation [8 ± 4% hOPCs are Ki67<sup>+</sup> at 8 weeks (4)], widespread cell death gives rise to a secondary inflammatory response due to the release of the intracellular alloantigens (50), which further exacerbates local inflammation and increases the likelihood of graft failure.

Previously, it was shown that injection of rat Schwann cells using a STH-improved cell survival as compared to saline in the context of a contusion induced SCI (8). However, cell transplantation in the context of congenital hypomyelinating brain is quite different from the local injury models like traumatic brain injury (TBI) and SCI, where the transplanted cells do not need to migrate to enhance regeneration. As a matter of fact, other cell types, such as MSCs, have been shown to be effective in the TBI (51–53) and SCI (54, 55) models. In contrast, our model of congenital hypomyelination is

directly relevant to human developmental myelin diseases such as Pelizaeus-Merzbacher disease. These genetic disorders are the result of global deficits in myelin formation and affect the whole brain and spinal cord. Therefore, the transplanted cells must migrate far from the site of injection, to occupy and myelinate the entire white matter. Thus far, only hOPCs have been demonstrated to do that, and Schwann cells are not appropriate as they are unable to migrate in CNS parenchyma due to the presence of astrocytes (56).

In this study, we hypothesized that a STH undergoing dynamic gel-sol transition when subjected to shear stress may protect hOPCs during injection and allow efficient migration of the transplanted hOPCs from the injection site to remyelinate the whole CC. To this end, we engineered a STH-based cell delivery system that can dissipate the shear stress as well as serve as a platform to immobilize pro-survival biological cues to enhance cell viability postinjection and subsequently the extent of remyelination. The two principal macromonomers of our STH are HA and PEG. HA is a primary component of the brain ECM (57), and PEG is a highly biocompatible, water-soluble polymer that supports cell growth and was found to reduce local glial scar invasion (58). Previous approaches used chemical cross-linking between HA and PEG to form hydrogels lacking the stress-relaxation capacity that is required to form an injectable hydrogel and may also affect the mechanical properties affecting stem cell fate decisions (40, 59, 60). The Burdick group harnessed host-guest assembly of βCD-adamantane to develop shear-thinning HA hydrogels, where the mechanical properties were controlled by altering the degree of modification of HA-CD and HA-Ad (18, 61). The resultant hydrogels were mechanically weak due to inherent reversibility of the host-guest interaction, making them ideally suited for injection into soft tissues. Formation of secondary covalent network via Michael addition chemistry or photocross-linking of methacrylate-modified HA was explored for prolonged stabilization of STHs (61).

Guided by previous studies (8, 40, 61), we sought to leverage βCD-adamantane assembly to design an injectable STH that is soft enough to mimic brain tissue and could accommodate pro-survival cues including growth factors (GFs). To achieve this goal, the STH was designed to: (i) incorporate host-guest dynamic bonds to enable cell delivery by injection while also protecting cells from shear stress by dissipating the injection force; and (ii) incorporate heparin as a means for immobilization of pro-survival cues and GFs via their HBD. Unlike previously reported design that relies on chemical conjugation of short peptides incorporating terminal cysteine residues to polymer backbone (61), inclusion of heparin in our design provided the opportunity to immobilize a broad spectrum of biological cues via HBDs. The attractive features of this design include (i) the hydrogel capacity to flow under shear, thereby protecting hOPCs from mechanical damage; (ii) the ability to conjugate pro-survival signals such as fibronectin and Lam-derived peptides under mild physiological conditions through Michael addition at neutral pH; (iii) as well as heparin-binding GFs, such as PDGF which may be necessary for hOPCs survival and proliferation; and (iv) the ability to tune their stiffness to match that of the host tissue. Injection of rat CG-4 or hOPCs demonstrated marked improvement of cell survival after injection through a fine needle in the presence of STH.

Oligodendrocytes express a variety of ECM binding integrins including α<sub>v</sub>β<sub>1</sub>, α<sub>v</sub>β<sub>3</sub>, α<sub>v</sub>β<sub>5</sub>, α<sub>v</sub>β<sub>8</sub>, and α<sub>6</sub>β<sub>1</sub> on their surface (62). They

also respond to a variety of soluble extracellular GFs including PDGF, fibroblast growth factor-2, insulin-like growth factor-1, neuregulin, and NT-3 regulating multiple stages of oligodendroglial development. Therefore, we developed a general framework to incorporate heparin-binding GFs and integrin ligands by synthesizing Hep-SH that was cross-linked into the STHs via  $\beta$ CD-Mal. In this study, we chose to incorporate PDGF-AA and the bidomain peptide, HBD-RGD5, into the STH to promote hOPC survival and proliferation posttransplantation (63, 64). This ECM-mimicking, GF-fortified STH provided protection from shear stress, as well as cell-adhesive and trophic support ultimately enhancing cell survival after transplantation and improving myelination. Incorporation of additional prosurvival and differentiation-promoting factors may further improve cell survival, as well as guide cell fate by preventing astrocytic differentiation of hOPCs leading to more efficient therapeutic outcome.

Moreover, although, in this study, we explored our STH system with hOPC transplantation in the brain, the same platform could be adopted for delivery of other cell types and other neurological disease indications. In addition, our work uses the use of human cells, which are directly translatable into the clinic; and demonstrating its feasibility in a congenital model of demyelination sets the stage to pursue this strategy in other models of multifocal human demyelinating disease, such as multiple sclerosis.

Last, while our study demonstrates promising results regarding the efficacy of the designed STHs in promoting cell survival and myelination in a mouse model, it is crucial to acknowledge certain limitations. For example, the use of newborn pups, which exhibit a different extracellular environment and may be more permissive for cell integration, may limit extrapolation to an adult model. However, hOPCs have been shown by others to engraft and migrate very efficiently when transplanted in adult mice (42). Animal models with an incomplete immune system may provide additional support to transplanted cell engraftment compared to scenarios with an intact immune system. However, it is envisioned that all human cell therapy will be accompanied by immunosuppressive regimens to prevent rejection. Furthermore, the use of a congenitally hypomyelinated model, where myelin formation is severely limited versus an immune-mediated demyelination in the context of multiple sclerosis may limit the generalizability of our findings. However, there is promising evidence that hOPCs are able to robustly remyelinate axons when transplanted into demyelinated lesions following cuprizone-mediated demyelination in adult mice (42). Addressing these limitations in future research endeavors would provide a more comprehensive understanding of the therapeutic potential and underlying mechanisms of STHs in the context of demyelinating diseases.

In conclusion, cell transplantation is a promising therapeutic strategy for the treatment of neurodegenerative and chronic demyelinating diseases such as multiple sclerosis. However, in vivo survival of transplanted stem cells is limited due to mechanical disruption of the cell membrane during injection, the absence of cell-guiding cues at lesion sites, and lack of appropriate signals that guide cell fate and promote cell function. Development of innovative shear-thinning and bioactive hydrogels was used to minimize cell death and provide trophic support for successful transplantation by methods that are less invasive than classical surgery, such as cell injection. These STHs exhibited high cell survival and enhanced myelination, indicating their potential for treatment of demyelinating diseases such as multiple sclerosis.

## MATERIALS AND METHODS

### Materials

Sodium hyaluronate (HA, 60 kDa) was purchased from Lifecore Biomedical (Chaska, MN). Heparin sodium salt from porcine intestinal mucosa (180 USP units/mg; catalog no. H3149-500KU, Sigma-Aldrich, St. Louis, MO), 8-arm  $\text{NH}_2$ -terminated polyethylene glycol (8-arm PEG- $\text{NH}_2$ , 40 kDa; catalog no. JKA8012, Sigma-Aldrich, St. Louis, MO), and EDC (98%) were obtained from Sigma-Aldrich (Atlanta, GA). 1-[Bis(dimethylamino)methylene]-1H-1,2,3-triazolo [4,5-b]pyridinium-3-oxide-hexafluorophosphate also known as HATU (99%) and 3-maleimido-propionic NHS ester were purchased from BroadPharm (San Diego, CA). Monosubstituted  $\beta$ CD- $\text{NH}_2$  (97%) was obtained from BOC Sciences (Shirley, NY). Adamantane-1-carboxylic acid (99%) and TCEP were received from Alfa Aesar (Chicago, IL). DTPDH was obtained from Frontier Scientific (catalog no. 50906-77-9, Sigma-Aldrich, St. Louis, MO). All chemicals were used as received without further purification.

### Synthesis of HA-SH

HA-SH (60 kDa) was synthesized by an amidation reaction between the carboxylic groups of HA and DTPDH in the presence of EDC as coupling agent at pH 4.75, followed by reductive cleavage of disulfide bonds using TCEP. Specifically, HA (1 g, 2.49 mmol  $\text{COOH}$ , 1.0 equiv.) and DTPDH (0.15 g, 0.62 mmol, 0.25 equiv.) were dissolved in deionized (DI) water at HA concentration (3 mg/ml), and the pH was adjusted to 4.75 using 1 M HCl. Afterward, EDC (0.12 g, 0.62 mmol, 0.25 equiv.) was added, and the reaction mixture was stirred for 4 hours. The pH was maintained at 4.75 during the reaction by adding 1 M HCl. Subsequently, TCEP (0.36 g, 1.24 mmol, 2.0 equiv. with respect to DTPDH) was added, and the reaction mixture was continued to stir for an additional 3 hours. HA-SH was purified by dialysis [molecular weight (MW) cutoff,  $\sim 10$  kDa] against salt water (pH 3.5, 100 mM NaCl) for 2 days followed by acidic water (pH adjusted to 3.5) for another 2 days and then freeze-dried to obtain the pure solid.

### Synthesis of 8-arm PEG-Ad

8-Arm adamantane-terminated PEG was synthesized by the coupling reaction between 8-arm PEG- $\text{NH}_2$  and adamantane-1-carboxylic acid in the presence of HATU as coupling agent and DIPEA as base. Specifically, 8-arm  $\text{NH}_2$ -terminated PEG (1.0 g,  $1 \times 10^{-4}$  mol, 1.0 equiv.  $\text{NH}_2$ ), adamantane-1-carboxylic acid (0.28 g, 1.6 mmol, 2.0 equiv.), and HATU (0.61 g, 1.6 mmol, 2.0 equiv.) were dissolved in 30 ml of  $N,N'$ -dimethylformamide (DMF) in a 100-ml glass-round flask. Then, DIPEA (0.41 g, 3.2 mmol, 4.0 equiv.) was added, and the reaction continued under stirring for 12 hours. The product was purified by precipitation from ether, followed by vacuum drying overnight. The dry product was dissolved in water, dialyzed against DI water for 3 days, and then freeze-dried to obtain a white solid, denoted as 8-arm PEG-Ad.

### Synthesis of $\beta$ CD-Mal

Mono-functionalized  $\beta$ -cyclodextrin maleimide was synthesized by reacting  $\beta$ CD- $\text{NH}_2$  with 3-maleimido-propionic NHS ester. Specifically,  $\beta$ CD- $\text{NH}_2$  (1 g,  $8.49 \times 10^{-4}$  mol, 1.0 equiv.) and 3-maleimido-propionic NHS ester (0.67 g,  $2.54 \times 10^{-3}$  mol, 3.0 equiv.) were added into a 50-ml round flask containing 8 ml of dry DMF. The reaction mixture was allowed to stir for 3 hours and

then purified by precipitation from acetone three times. The pure product was collected after vacuum drying for 24 hours and denoted as  $\beta$ CD-Mal.

### Synthesis of Hep-SH

Heparin sodium salt (1.0 g,  $8.3 \times 10^{-2}$  mmol) and DTPDH (0.10 g, 0.42 mmol) were dissolved in DI water at a heparin concentration of 5 mg/ml. The pH was adjusted to 4.75 using 1 M HCl. Afterward, EDC ( $8.0 \times 10^{-2}$  g, 0.42 mmol) was added, and the reaction proceeded under stirring for 3 h. The pH was kept at 4.75 during the reaction by addition of 1 M HCl. Then, TCEP (0.24 g, 8.4 mmol) was added, and the reaction mixture was stirred for an additional 3 hours without pH adjustment. Hep-SH was purified by dialysis (MW cut-off,  $\sim 10$  kDa) against salt water (pH 3.5, 100 mM NaCl) for 2 days, followed by acidic water (pH adjusted to 3.5) for another 2 days, and then freeze-dried to obtain the product as a white solid.

### Development of supramolecular STHs

Injectable STHs of tunable stiffness and bioactivity were prepared as follows. First, 8-arm PEG-Ad was reconstituted in Hepes buffer (pH 7.4) to achieve 20.0 wt % concentration. Then,  $\beta$ CD-Mal was added at  $\beta$ CD/adamantane stoichiometric ratio of 1:1 to form SMP containing terminal maleimide groups, termed as SMP-Mal, through host-guest complexation between  $\beta$ CD and adamantane motifs. Second, HA-SH and Hep-SH were reconstituted separately in Hepes solution (pH 7.4) to achieve 4.0 and 8.0 wt %, respectively. The pH of the solutions was adjusted to 7.4 using 1 M NaOH. Last, STHs were prepared by mixing different volumes of the above solutions at room temperature (RT). Excess thiol groups were blocked by using 2-hydroxyethyl maleimide to avoid disulfide cross-linking. Last, recombinant HBD-RGD5 peptide and/or PDGF-AA were allowed to bind to Hep-SH at 37°C for 2 hours before mixing with SMP-Mal followed by addition of HA-SH. Three samples were prepared and denoted as STH-1 (total solid, 6.0 wt %; HA<sub>2wt%</sub>SMP<sub>3.3wt%</sub>), STH-2 (total solid, 8.7 wt %; HA<sub>1.3wt%</sub>SMP<sub>6.6wt%</sub>), and STH-3 (total solid, 11.0 wt %; HA<sub>0.66wt%</sub>SMP<sub>10wt%</sub>) (table S1).

### Measurements

<sup>1</sup>H NMR spectra were performed on a Varian INOVA-500 spectrometer at RT. The samples were dissolved in D<sub>2</sub>O or deuterated dimethyl sulfoxide (DMSO-d<sub>6</sub>) containing 1 vol % tetramethylsilane as the internal standard. The host-guest complexation between 8-arm PEG-Ad and  $\beta$ CD-Mal was confirmed by 2D ROESY NMR using D<sub>2</sub>O as solvent. The sample was prepared by dissolving both components in D<sub>2</sub>O at CD/adamantane molar ratio of 1:1.

The degree of substitution of HA-SH was obtained from the <sup>1</sup>H NMR spectrum using the integration of CH<sub>3</sub> group of HA at 1.89 ppm and CH<sub>2</sub>SH at 2.78 ppm. Likewise, the degree of functionalization of Hep-SH was quantified from the <sup>1</sup>H NMR analysis of a sample spiked with maleic acid as internal standard. The degree of thiolation was calculated from the resonance intensity of CH<sub>2</sub>SH at 2.78 ppm and that of maleic anhydride at 6.31 ppm. Mass analysis of monosubstituted  $\beta$ CD-Mal was conducted on Bruker Solarix 12 T Fourier Transform Ion Cyclotron Resonance Mass Spectrometer, equipped with electrospray ionization.

Oscillatory rheology was performed on a stress-controlled rheometer (HR 30, TA Instruments) using 20-mm parallel plate geometry to measure the viscoelastic properties of each hydrogel. STHs were loaded on the rheometer immediately after mixing, and a

humidity chamber was used to avoid dehydration. Dynamic frequency sweep from 0.1 to 10 Hz at constant 0.5% strain was conducted at RT, and the storage modulus (G') and loss modulus (G'') were recorded. Shear-thinning and self-healing behavior of hydrogels was assessed by viscosity measurements under time sweep mode at alternating low and high shear rates of 0.1 and 10 s<sup>-1</sup>, respectively, each for 30 s and for a total of 150 s. For stress-relaxation test, constant strain (10%) was applied, and the relaxation modulus was monitored over time. Stress-relaxation  $t_{1/2}$  was calculated as the time required for the relaxation modulus to reach half of its initial value.

### STH degradation and measurement of the released

#### HA content

Three different STH formulations (STH-1, STH-2, and STH-3) were prepared by varying the ratios (% w/v) of component 1 (HA-SH) and component 2 (SMP-Mal). One hundred microliters of each hydrogel was placed at the bottom of a 96-well plate in triplicates and centrifuged softly for 15 s at 300g in an Eppendorf centrifuge (model #5810) equipped with a swinging bucket rotor followed by the addition of 200  $\mu$ l of PBS on top of the gel. The plate was incubated at 37°C, and 50  $\mu$ l of the supernatant was withdrawn daily for 7 days followed by immediate addition of fresh 50  $\mu$ l of PBS. Degradation of the STH was determined by measuring the content of released HA (from component 1) in the supernatant solution. The  $\beta$ (1,4)-glycosidic bond of the structural unit of HA as shown in Fig. 1 (ii) was cleaved enzymatically to yield glucuronic acid and NAG, which was assayed colorimetrically using Ehrlich's reagent as described by Sall and Féraud (29). Briefly, appropriate concentrations (0.1 to 5.0%, w/v) of freshly reconstituted HA-SH solution was used as the standard for the colorimetric determination of NAG content. Briefly, 50  $\mu$ l of standard or sample solution was incubated with 50  $\mu$ l of hyaluronidase (6080 U/ml; Sigma-Aldrich, catalog no. H3506) solution in a 1.5-ml tube at 37°C for 5 min. The enzymatic reaction was stopped by the addition of 50  $\mu$ l of potassium tetraborate solution (0.8 M, pH of 9.1, Acros Organics, catalog no. 259572500), immediately vortexed, and placed in a boiling water bath for 3 min. Once the tubes were cooled down to RT, 150  $\mu$ l of Ehrlich's solution (1:10 dilution in glacial acetic acid, Sigma-Aldrich, catalog no. 03891) was added and kept at 37°C for 5 min to allow color development. Then, the contents were centrifuged at high speed for 30 s followed by immediate transfer of 100  $\mu$ l of solution to a 96-well plate. The absorbance was recorded at 585 nm using a Biotek Synergy 4 plate reader as suggested by the manufacturer.

### Cloning and production of the recombinant fusion proteins

The core sequence of the two fusion proteins, Hep2-(GGGS-HIPREDVDYH)<sub>5</sub> and Hep2-(GGGS-GRGDS)<sub>5</sub>, consists of two parts: (i) Hep2, the second HBD of fibronectin; (ii) R5, five tandem repeats, each composed of a flexible linker motif, GGGS followed by a peptide HIPREDVDYH or GRGDS, that are known for binding preferably to integrin  $\alpha_4\beta_1$  and  $\alpha_v\beta_1$ , respectively (65). The Hep2 domain was cloned by reverse transcription polymerase chain reaction from the second HBD of fibronectin using cloning primers (table S3) containing the Bam HI and Xho I cutting sites and inserted in the pET28a-expressing vector. The R5 sequence of REDV-containing cutting sites Hind III and Xho I was purchased from Invitrogen and cloned next to the H2 in the pET28a expression vector as described previously by Nasiri *et al.* (66). The cloning

primers for the R5 sequence of RGD containing the cutting sites Hind III and Xho I were purchased from Invitrogen in two short fragments (table S3). Following the ligation of the two fragments, they were cloned by inserting them next to the HBD domain of the pET28a-expressing vector as described by Podder *et al.* (67).

The bidomain peptides, HBD-REDV5 and HBD-RGD5, were produced in the bacterial strain *Escherichia coli* BL21-DE3-pLysis. Specifically, bacteria were expanded until the optical density reaches a value of 0.7 and then induced with 0.1 mM isopropyl  $\beta$ -D-1-thiogalactopyranoside (Sigma-Aldrich) for protein production overnight at 22°C and 240 rpm. The following day, the bacteria were centrifuged at 4000 rpm for 20 min, and the pellets were resuspended in lysis buffer [500 mM NaCl (VWR) in 1× PBS (pH 7.4), containing lysozyme (1 mg/ml; Sigma-Aldrich), 1% Triton X-100 (Sigma-Aldrich), and 1 mM phenylmethylsulfonyl fluoride (Sigma-Aldrich) as protease inhibitor stirred for 1 hour at RT followed by sonication for 10 cycles with 50% intensity, 30 s on/30 s off. The soluble protein was obtained by ultracentrifugation of the sonicated lysate at 50,000g for 15 min using the Avanti high-performance centrifuge (Beckman Coulter Inc., Indianapolis, IN, USA). Fusion proteins were then purified using HisTrap HP Column (Cytiva, Uppsala, Sweden) following the manufacturer's instructions. The purity of the collected protein was tested using 10% SDS–polyacrylamide gel electrophoresis, where the bidomain peptides were apparent at an MW of ~40 kDa. Bradford assay was used to determine the final protein concentration.

### Cell culture

Fetal brain tissues (17 to 22 weeks gestational age) were obtained from Advanced Bioscience Resources with informed consent from all donors. All research was performed according to relevant guidelines and was reviewed by the University at Buffalo Research Subjects Institutional Review Board. Brain tissues were minced and dissociated using papain and deoxyribonuclease always within 2 hours of extraction as described previously by Conway *et al.* (68). CD140a/PDGFR $\alpha$ <sup>+</sup> cells (hOPCs) were magnetically sorted as described (69). Cells were seeded on poly-L-ornithine (PLO; Sigma-Aldrich, catalog no. P3655)–and Lam (Invitrogen, catalog no. 23017-015)–coated plates at a density of 50,000/ml and maintained in the oligodendrocyte progenitor state by supplementing the neural differentiation (ND) medium with PDGF-AA (20 ng/ml; PeproTech, catalog no. 100-13A) and NT-3 (5 ng/ml; PeproTech, catalog no. 450-03). For preliminary evaluation of the different STH compositions and migration assay, CG-4 rat OPCs were cultured on PDL-coated flasks in ND media supplemented with PDGF-AA (10 ng/ml) and basic fibroblast growth factor (bFGF; 10 ng/ml; ISOkine, catalog no. 01-A01110-0100). The ND medium consists of a 1:1 mixture of Dulbecco's Modified Eagle's Medium (DMEM)/F12 (VWR, catalog no. 45000-350) and neurobasal medium (Invitrogen, catalog no. 21103-049) with Hepes (7.5 mM), sodium pyruvate (1 mM; VWR, catalog no. 10128-7640), L-glutamine (2 mM; VWR, catalog no. VWRL0131-0100), penicillin/streptomycin (1×; VWR, catalog no. 97063-708), B27 supplement (1×; Invitrogen, catalog no. 17504044), N2 supplement (1×; Invitrogen, catalog no. 17502048), transferrin (100  $\mu$ g/ml), insulin (5  $\mu$ g/ml), putrescine (16.11  $\mu$ g/ml), progesterone (66.3 ng/ml; MilliporeSigma, catalog no. P6149), selenite (55.2 ng/ml; MilliporeSigma, catalog no. S9133), trace elements B (1×; VWR, catalog no. 25-022-CI), and N-acetyl cysteine (5  $\mu$ g/ml; Sigma-Aldrich, catalog no. A8199).

### Cell viability following injection

CG-4 and/or hOPCs were trypsinized and resuspended in the appropriate volume of HBSS or different STH formulations to a final cell density of 100,000/ $\mu$ l. The cell suspensions were drawn in and injected out (0.1  $\mu$ l every 5 s) through a Hamilton syringe fitted with pulled glass needle (ID: 100 to 200  $\mu$ m equivalent to 28- to 32-G needle). Following injection, the STHs were promptly disrupted by mixing in media rich in free cyclodextrin (unmodified, free cyclodextrin, 30 mM) which competes for the  $\beta$ CD-Mal (cyclodextrin-maleimide), leading to an immediate breakdown of the STH structure and releasing cells. Subsequently, the cells were diluted in appropriate volume of cyclodextrin-rich OPC media to a concentration of 50,000 cells/ml and seeded into a 48-well plate. After 3 hours, cell survival was tested by staining with a live/dead assay kit (Invitrogen, catalog no. L3224) following the manufacturer's protocol and imaged using a Zeiss Axio Observer Z1 inverted microscope with an ORCA-ER charge-coupled device (CCD) camera (Hamamatsu, Japan).

### Cell survival within the hydrogel

Following trypsinization, the hOPCs (final concentration: 1000/ $\mu$ l) were resuspended in appropriate volume of STH component 1 (HA-SH) and then mixed with component 2 (SMP-Mal) at different ratios to form three different STH formulations. SMP-Mal was conjugated with the biological cues (HBD-RGD5 and PDGF-AA). After 48 hours in culture, cell survival was assessed using the live/dead assay (Invitrogen, catalog no. L3224). Images were captured in three random fields at  $\times$ 4 and  $\times$ 40 magnification using an IX83 microscope (Olympus) and analyzed with Fiji software.

### Measurements of cell spreading and proliferation

To evaluate the effect of bidomain peptides on cell proliferation, hOPCs were trypsinized and seeded either on PLO-Lam (served as control)–coated or peptide-functionalized 48-well tissue culture plates at a density of 50,000 cells/ml in ND media supplemented with PDGF-AA (20 ng/ml) and NT-3 (5 ng/ml). For the immobilization of heparin-binding peptides, the plates were first coated with positive (+)ly charged PLO (0.1 mg/ml) solution for >1 hour and then by negative (–)ly charged heparin (2.0 mg/ml; Sigma-Aldrich, catalog no. H4784) solution for >3 hours at 37°C followed by overnight incubation with different concentrations of bidomain peptides (HBD-RGD5 or HBD-REDV5). To measure DNA synthesis during cell proliferation after 48 hours post-seeding, cells were pretreated with a DNA nucleoside (thymidine) analog, 5-ethynyl-2'-deoxyuridine known as EdU (10  $\mu$ M; VWR, catalog no. TCE1057) for 8 hours before fixing using 4% paraformaldehyde solution. To evaluate the effect of PDGF-AA on cell proliferation, hOPCs were seeded on control (PLO-Lam) plates at 50,000 cells/ml in PDGF-AA and NT-3 supplemented ND media. The next day, media was changed to GF-free ND media for 24 hours, and then the cells were introduced to various concentrations of PDGF-AA and cultured for the next 24 hours with a terminal 8-hour pulse of EdU (10  $\mu$ M) before fixing. Cells were visualized by staining with a Click-iT EdU Alexa Fluor 488 imaging kit (Invitrogen, catalog no. 10337) as per the manufacturer's instruction. To label the nuclei, cells were costained with 4',6-diamidino-2-phenylindole (DAPI; Sigma-Aldrich, catalog no. D8417).

To evaluate the effect of recombinantly designed bidomain peptides on cell integrin binding, plates were coated with PDL, HBD-REDV5, and HBD-RGD5 as described above. Then, the CG-4 rat OPCs were plated at 50,000/ml on different substrates in ND medium supplemented with PDGF-AA (10 ng/ml) and bFGF (10 ng/ml). The cells were cultured for 48 hours before fixing.

### In vitro differentiation of the hOPCs

To evaluate the effect of bidomain fusion peptides on hOPC differentiation, cells were seeded either on PLO-Lam (control) or peptide-coated plates at 50,000/ml in PDGF-AA and NT-3 supplemented ND media as described above. After 24 hours, the GFs were removed to initiate cell differentiation. Ninety-six hours following GF removal, the hOPCs were live-stained with the O4 immunoglobulin M hybridoma supernatant (1:20; gift from J. Goldman, Columbia University) 30 min before fixing with 4% paraformaldehyde, followed by incubation with secondary antibody for 1 hour at RT. The proportion of differentiated cells was quantified by measuring the O4<sup>+</sup> cells from three fetal donors ( $n = 3$ ).

To determine the differentiation behavior of the hOPCs in 3D, trypsinized cells were resuspended in appropriate volume of STH component 1 (HA-SH) and then mixed with component 2 (SMP-Mal) at different ratios to form three STH formulations (cell density: 1000/ $\mu$ l). After 96 hours in medium without mitogens, oligodendroglial differentiation was evaluated by immunostaining with the O4 antibody as described above. Images were captured in three random fields at  $\times 4$  and  $\times 40$  magnification using an IX83 microscope (Olympus) and analyzed with Fiji software.

### Migration assay

PDL-coated transwell inserts (Corning, catalog no. 3422; membrane diameter: 6.5 mm, pore size = 8  $\mu$ m) were coated either with STH only or STH immobilized with variable concentrations of HBD-RGD5 fusion peptide. The CG-4 rat OPCs (50,000/ml in ND medium only) were then cultured on the respective hydrogel substrates in the upper chamber of the inserts. PDGF-AA was introduced at 50 ng/ml in the ND medium in the lower chamber, and cells were allowed to migrate for 16 hours through the hydrogel and subsequently reach the opposite side of the PDL-coated membrane. The cells were then fixed with a 4% paraformaldehyde, and their nuclei were stained with DAPI. Any residual STH and cells were scraped from the top surface of the membrane insert before imaging. Only the cells on the opposite side (migrated) of the inserts were counted, and the results were reported as the percentage of cell migration.

### Mice transplantation

All animal experiments were performed according to the protocols (PMY43099Y) approved by the University at Buffalo Institutional Animal Care and Use Committee. Two types of mouse models were used in this study. Immunocompromised NSG mice (the Jackson Laboratory; strain 005557) were used to evaluate cell survival postinjection, and immunocompromised, hypomyelinating *shiverer/rag2* mice (a gift from S. A. Goldman, University of Rochester) was used to analyze the in vivo myelination capability of the hOPCs with STH alone or with immobilized biological cues. Frozen CD140a<sup>+</sup> hOPCs were cultured for 2 to 3 days in ND medium

supplemented with PDGF-AA (20 ng/ml) and NT-3 (5 ng/ml) before surgery. Before transplantation, trypsinized hOPCs were resuspended either in HBSS, STH, or STH with immobilized biological cues at a concentration of 100,000/ $\mu$ l as described previously by Abiraman *et al.* (28). Briefly, 2- to 3-day old newborn pups were anesthetized using hypothermia, and 50,000 cells were injected unilaterally (in the NSG mice) and bilaterally (*shiverer* mice) at a depth of 1.1 mm into the rostral (~2.5 mm posterior to the bregma) CC of the brain. Pulled glass pipettes of 100- to 200- $\mu$ m ID were used to inject the cells directly through the skull into the presumptive target CC region. All the injections were made in an identical manner for both control and STH groups. Animals were euthanized after 6 weeks (NSG mice) or 12 weeks (*shiverer* mice) by transcardial perfusion with 0.9% (w/v) saline followed by a 4% (w/v) formaldehyde solution under deep anesthesia.

To assess the distribution of the hydrogel within the brain postinjection, we conjugated Cy5.5-maleimide [Lumiprobe, catalog no. 47080\_ dye:HA (w/w) = 1:84] to HA-SH before mixing with SMP-Mal to create the fluorescently labeled STH-2. STH-2-Cy5.5 was transplanted into *shiverer* pups that were then euthanized on days 3, 7, and 14 postinjection for evaluation of the hydrogel location and distribution.

### Histological analysis of brain sections

Cryopreserved mouse forebrains were cut as 16- $\mu$ m-thick sections and sampled every 160  $\mu$ m on the positively charged glass slides. Immunohistochemistry was performed as described previously by Welliver *et al.* (70). Briefly, human cells (hOPCs) were identified first by staining with mouse anti-hNA (1:400; MilliporeSigma, catalog no. MAB1281). The brain section corresponding to the highest count of hNA<sup>+</sup> cells for each animal was assigned as the point of injection, and the rest of the rostral to caudal data points was plotted accordingly in the X axis (Figs. 6E and 7C).

Myelination was evaluated by rat anti-MBP antibody at 1:200 (Abcam, catalog no. ab7349). To determine the early and mature (differentiated) oligodendrocyte lineage, goat OLIG2 (R&D Systems, catalog no. AF2418) and CC1 (MilliporeSigma, catalog no. OP80) antibodies were used. Astrocytic and early neural progenitor state was evaluated by mouse GFAP (BioLegend, catalog no. 837201) and rabbit SOX2 (Invitrogen, catalog no. 48-1400) primary antibody, respectively. All secondary antibodies (Invitrogen, Alexa Fluor 488, Alexa Fluor 568, and Alexa Fluor 647) were used at 1:500 dilution. Images of the entire coronal sections were captured under matching conditions using the 10 $\times$  objective of a Zeiss Axio Observer Z1 inverted microscope with an ORCA-ER CCD camera (Hamamatsu, Japan). The images were captured using a fixed exposure time for each fluorescent dye for all the samples. MBP<sup>+</sup> area was assessed as the percentage of total area of the CC in the region of interest (ROI). Since the hOPCs tend to migrate from one side of the brain to the other (left to right and vice versa), the ROI was defined by drawing a region of approximately 0.2 mm<sup>2</sup> in the CC around the injection point. For OLIG2, CC1, and GFAP counting, three different sections (320  $\mu$ m apart from each other) were analyzed. At least three different regions spanning left, midline, and right of the CC were analyzed for each brain section. For counting, data from four to five sections were averaged to generate a single data point for each animal. Confocal images were obtained by a white light laser scanning Leica Stellaris 5 (Leica Microsystems, Wetzlar, Germany) with a 20 $\times$  objective, and the z-stack depth was

within 15  $\mu\text{m}$  (step = 1  $\mu\text{m}$ ). Analysis of the fluorescence images was done using the ImageJ software.

### RNA sequencing

Human fetal CD140a<sup>+</sup> OPCs were cultured under proliferative conditions using serum-free media supplemented with PDGF-AA (20 ng/ml) and NT-3 (5 ng/ml). The hOPCs isolated from 20- to 21-week-old, aborted fetuses ( $n = 2$ ) were used to collect the RNA. The two RNA samples analyzed were derived from replicate hOPC cultures originating from a mixture of three biologically distinct human samples. RNA was extracted from hOPCs cultured either at low density (initial density 20,000 cells/ml and extracted 60 hours postseeding) or at high density (initially seeded at 50,000 cells/ml and allowed to reach confluency, ~7 days post-seeding). RNA extraction and first-strand synthesis were performed as described previously (68). RNA-seq was performed (71) at the University at Buffalo sequencing core on an Illumina HiSeq2500 using 100 cycle paired-end sequencing. Sequences were aligned to the UCSC Hg19 mouse genome using Tophat (v2.1.1), and counts per gene were determined using htseq (v0.6.1). R/Bioconductor was used for subsequent analysis. Following loading of read counts using DESeq2, FPKM were calculated.

### Statistical analysis

All statistical analyses were performed using GraphPad Prism software. Data were compared by Student's  $t$  test, one-way analysis of variance (ANOVA) followed by post hoc test, where appropriate. The data are expressed as mean  $\pm$  SD; \* $P < 0.05$ , \*\* $P < 0.005$ , \*\*\* $P < 0.0005$ , and \*\*\*\* $P < 0.0001$  were considered statistically significant.

### Supplementary Materials

#### This PDF file includes:

Figs. S1 to S14  
Tables S1 to S3  
Legend for movie S1

#### Other Supplementary Material for this manuscript includes the following:

Movie S1

### REFERENCES AND NOTES

- V. Tepavčević, C. Lubetzki, Oligodendrocyte progenitor cell recruitment and remyelination in multiple sclerosis: The more, the merrier? *Brain* **145**, 4178–4192 (2022).
- S. A. Goldman, J. N. Mariani, P. M. Madsen, Glial progenitor cell-based repair of the dysmyelinated brain: Progression to the clinic. *Semin. Cell Dev. Biol.* **116**, 62–70 (2021).
- M. S. Windrem, S. J. Schanz, M. Guo, G. F. Tian, V. Washco, N. Stanwood, M. Rasband, N. S. Roy, M. Nedergaard, L. A. Havton, S. Wang, S. A. Goldman, Neonatal chimerization with human glial progenitor cells can both remyelinate and rescue the otherwise lethally hypomyelinated shiverer mouse. *Cell Stem Cell* **2**, 553–565 (2008).
- F. J. Sim, C. R. McClain, S. J. Schanz, T. L. Protack, M. S. Windrem, S. A. Goldman, CD140a identifies a population of highly myelinogenic, migration-competent and efficiently engraving human oligodendrocyte progenitor cells. *Nat. Biotechnol.* **29**, 934–941 (2011).
- P. Douvaras, J. Wang, M. Zimmer, S. Hanchuk, M. A. O'Bara, S. Sadiq, F. J. Sim, J. Goldman, V. Fossati, Efficient generation of myelinating oligodendrocytes from primary progressive multiple sclerosis patients by induced pluripotent stem cells. *Stem. Cell Rep.* **3**, 250–259 (2014).
- B. A. Aguado, W. Mulyasmita, J. Su, K. J. Lampe, S. C. Heilshorn, Improving viability of stem cells during syringe needle flow through the design of hydrogel cell carriers. *Tissue Eng. Part A* **18**, 806–815 (2011).
- M. Zhang, D. Methot, V. Poppa, Y. Fujio, K. Walsh, C. E. Murry, Cardiomyocyte grafting for cardiac repair: Graft cell death and anti-death strategies. *J. Mol. Cell. Cardiol.* **33**, 907–921 (2001).
- L. M. Marquardt, V. M. Doulames, A. T. Wang, K. Dubbin, R. A. Suhar, M. J. Kratochvil, Z. A. Medress, G. W. Plant, S. C. Heilshorn, Designer, injectable gels to prevent transplanted Schwann cell loss during spinal cord injury therapy. *Sci. Adv.* **6**, eaaz1039 (2020).
- C. D. Plant, G. W. Plant, "Schwann cell transplantation methods using biomaterials" in *Schwann Cells: Methods and Protocols*, P. V. Monje, H. A. Kim, Eds. (Springer, 2018), pp. 439–453.
- M. Koda, Y. Someya, Y. Nishio, R. Kadota, C. Mannoji, T. Miyashita, A. Okawa, A. Murata, M. Yamazaki, Brain-derived neurotrophic factor suppresses anoikis-induced death of Schwann cells. *Neurosci. Lett.* **444**, 143–147 (2008).
- R. C. Op 't Veld, X. F. Walboomers, J. A. Jansen, F. A. D. T. G. Wagener, Design considerations for hydrogel wound dressings: Strategic and molecular advances. *Tissue Eng. Part B Rev.* **26**, 230–248 (2020).
- M. Desgres, P. Menasché, Clinical translation of pluripotent stem cell therapies: Challenges and considerations. *Cell Stem Cell* **25**, 594–606 (2019).
- J. Boltze, M. M. Modo, R. W. Mays, A. Taguchi, J. Jolkonen, S. I. Savitz, STEPS 4 Consortium, Stem cells as an emerging paradigm in stroke 4: Advancing and accelerating preclinical research. *Stroke* **50**, 3299–3306 (2019).
- Z. May, R. Kumar, T. Fuehrmann, R. Tam, K. Vulic, J. Forero, A. Lucas Osma, K. Fenrich, P. Assinck, M. J. Lee, A. Moulson, M. S. Shoichet, W. Tetzlaff, J. Biernaskie, K. Fouad, Adult skin-derived precursor Schwann cell grafts form growths in the injured spinal cord of Fischer rats. *Biomed. Mater.* **13**, 034101 (2018).
- M. Guvendiren, H. D. Lu, J. A. Burdick, Shear-thinning hydrogels for biomedical applications. *Soft Matter* **8**, 260–272 (2012).
- M. Guo, M. Jiang, S. Pispas, W. Yu, C. Zhou, Supramolecular hydrogels made of end-functionalized low-molecular-weight PEG and  $\alpha$ -cyclodextrin and their hybridization with SiO<sub>2</sub> nanoparticles through host-guest interaction. *Macromolecules* **41**, 9744–9749 (2008).
- C. B. Highley, C. B. Rodell, J. A. Burdick, Direct 3D printing of shear-thinning hydrogels into self-healing hydrogels. *Adv. Mater.* **27**, 5075–5079 (2015).
- C. B. Rodell, A. L. Kaminski, J. A. Burdick, Rational design of network properties in guest-host assembled and shear-thinning hyaluronic acid hydrogels. *Biomacromolecules* **14**, 4125–4134 (2013).
- D. Wang, Y. Xia, D. Zhang, X. Sun, X. Chen, S. Oliver, S. Shi, L. Lei, Hydrogen-bonding reinforced injectable hydrogels: Application as a thermo-triggered drug controlled-release system. *ACS Appl. Polym. Mater.* **2**, 1587–1596 (2020).
- S. Liu, D. Qi, Y. Chen, L. Teng, Y. Jia, L. Ren, Quadruple hydrogen bonds and thermo-triggered hydrophobic interactions generate dynamic hydrogels to modulate transplanted cell retention. *Biomater. Sci.* **7**, 1286–1298 (2019).
- L. Zhao, M. D. Weir, H. H. K. Xu, An injectable calcium phosphate-alginate hydrogel-umbilical cord mesenchymal stem cell paste for bone tissue engineering. *Biomaterials* **31**, 6502–6510 (2010).
- A. K. Gaharwar, R. K. Avery, A. Assmann, A. Paul, G. H. McKinley, A. Khademhosseini, B. D. Olsen, Shear-thinning nanocomposite hydrogels for the treatment of hemorrhage. *ACS Nano* **8**, 9833–9842 (2014).
- N. M. B. Smeets, M. Patenaude, D. Kinio, F. M. Yavitt, E. Bakaic, F.-C. Yang, M. Rheinstädter, T. Hoare, Injectable hydrogels with in situ-forming hydrophobic domains: Oligo(d,l-lactide) modified poly(oligoethylene glycol methacrylate) hydrogels. *Polym. Chem.* **5**, 6811–6823 (2014).
- L. Meng, C. Shao, C. Cui, F. Xu, J. Lei, J. Yang, Autonomous self-healing silk fibroin injectable hydrogels formed via surfactant-free hydrophobic association. *ACS Appl. Mater. Interfaces* **12**, 1628–1639 (2020).
- Z. Wei, J. H. Yang, J. Zhou, F. Xu, M. Zrínyi, P. H. Dussault, Y. Osada, Y. M. Chen, Self-healing gels based on constitutional dynamic chemistry and their potential applications. *Chem. Soc. Rev.* **43**, 8114–8131 (2014).
- S. A. Goldman, M. Nedergaard, M. S. Windrem, Glial progenitor cell-based treatment and modeling of neurological disease. *Science* **338**, 491–495 (2012).
- S. Wang, J. Bates, X. Li, S. Schanz, D. Chandler-Militello, C. Levine, N. Maherali, L. Studer, K. Hochedlinger, M. Windrem, S. A. Goldman, Human iPSC-derived oligodendrocyte progenitor cells can myelinate and rescue a mouse model of congenital hypomyelination. *Cell Stem Cell* **12**, 252–264 (2013).
- K. Abiraman, S. U. Pol, M. A. O'Bara, G.-D. Chen, Z. M. Khaku, J. Wang, D. Thorn, B. H. Vedia, E. C. Ekwegbalu, J.-X. Li, R. J. Salvi, F. J. Sim, Anti-muscarinic adjunct therapy accelerates functional human oligodendrocyte repair. *J. Neurosci.* **35**, 3676–3688 (2015).
- I. Sall, G. Féraud, Comparison of the sensitivity of 11 crosslinked hyaluronic acid gels to bovine testis hyaluronidase. *Polym. Degrad. Stab.* **92**, 915–919 (2007).
- J. R. E. Fraser, T. C. Laurent, U. B. G. Laurent, Hyaluronan: Its nature, distribution, functions and turnover. *J. Intern. Med.* **242**, 27–33 (1997).
- J. W. McDonald, X. Z. Liu, Y. Qu, S. Liu, S. K. Mickey, D. Turetsky, D. I. Gottlieb, D. W. Choi, Transplanted embryonic stem cells survive, differentiate and promote recovery in injured rat spinal cord. *Nat. Med.* **5**, 1410–1412 (1999).

32. M. Iwasaki, J. T. Wilcox, Y. Nishimura, K. Zweckberger, H. Suzuki, J. Wang, Y. Liu, S. K. Karadimas, M. G. Fehlings, Synergistic effects of self-assembling peptide and neural stem/progenitor cells to promote tissue repair and forelimb functional recovery in cervical spinal cord injury. *Biomaterials* **35**, 2617–2629 (2014).
33. C. S. Barros, T. Nguyen, K. S. Spencer, A. Nishiyama, H. Cognato, U. Müller, Beta1 integrins are required for normal CNS myelination and promote AKT-dependent myelin outgrowth. *Development* **136**, 2717–2724 (2009).
34. R. W. O'Meara, J. P. Michalski, R. Kothary, Integrin signaling in oligodendrocytes and its importance in CNS myelination. *J. Signal. Transduct.* **2011**, 1–11 (2011).
35. B. LaFoya, J. A. Munroe, A. Miyamoto, M. A. Detweiler, J. J. Crow, T. Gazdik, A. R. Albig, Beyond the Matrix: The many non-ECM ligands for integrins. *Int. J. Mol. Sci.* **19**, 449 (2018).
36. M. Benito-Jardón, N. Strohmeier, S. Ortega-Sanchís, M. Bharadwaj, M. Moser, D. J. Müller, R. Fässler, M. Costell,  $\alpha$ -Class integrin binding to fibronectin is solely mediated by RGD and unaffected by an RGE mutation. *J. Cell Biol.* **219**, (2020).
37. F. Danhier, A. Le Breton, V. Pr at, RGD-based strategies to target alpha(v) beta(3) integrin in cancer therapy and diagnosis. *Mol. Pharm.* **9**, 2961–2973 (2012).
38. W. Baron, H. Cognato, C. French-Constant, Integrin-growth factor interactions as regulators of oligodendroglial development and function. *Glia* **49**, 467–479 (2005).
39. M. Segel, B. Neumann, M. F. E. Hill, I. P. Weber, C. Viscomi, C. Zhao, A. Young, C. C. Agle, A. J. Thompson, G. A. Gonzalez, A. Sharma, S. Holmqvist, D. H. Rowitch, K. Franze, R. J. M. Franklin, K. J. Chalut, Niche stiffness underlies the ageing of central nervous system progenitor cells. *Nature* **573**, 130–134 (2019).
40. X. Li, X. Liu, L. Cui, C. Brunson, W. Zhao, N. R. Bhat, N. Zhang, X. Wen, Engineering an in situ crosslinkable hydrogel for enhanced remyelination. *FASEB J.* **27**, 1127–1136 (2013).
41. K. Sinha, S. Karimi-Abdolrezaee, A. A. Velumian, M. G. Fehlings, Functional changes in genetically dysmyelinated spinal cord axons of shiverer mice: Role of juxtaparanodal Kv1 family K<sup>+</sup> channels. *J. Neurophysiol.* **95**, 1683–1695 (2006).
42. M. S. Windrem, S. J. Schanz, L. Zou, D. Chandler-Millette, N. J. Kuypers, M. Nedergaard, Y. Lu, J. N. Mariani, S. A. Goldman, Human glial progenitor cells effectively remyelinate the demyelinated adult brain. *Cell Rep.* **31**, 107658 (2020).
43. Y. Wang, J. H. Piao, E. C. Larsen, Y. Kondo, I. D. Duncan, Migration and remyelination by oligodendrocyte progenitor cells transplanted adjacent to focal areas of spinal cord inflammation. *J. Neurosci. Res.* **89**, 1737–1746 (2011).
44. S. A. Goldman, Stem and progenitor cell-based therapy of the central nervous system: Hopes, hype, and wishful thinking. *Cell Stem Cell* **18**, 174–188 (2016).
45. A. Parisi-Amon, W. Mulyasmita, C. Chung, S. C. Heilshorn, Protein-engineered injectable hydrogel to improve retention of transplanted adipose-derived stem cells. *Adv. Healthc. Mater.* **2**, 428–432 (2013).
46. I. Kutschka, I. Y. Chen, T. Kofidis, T. Arai, G. von Degenfeld, A. Y. Sheikh, S. L. Hendry, J. Pearl, G. Hoyt, R. Sista, P. C. Yang, H. M. Blau, S. S. Gambhir, R. C. Robbins, Collagen matrices enhance survival of transplanted cardiomyoblasts and contribute to functional improvement of ischemic rat hearts. *Circulation* **114**, 1167–1173 (2006).
47. T. Freyman, G. Polin, H. Osman, J. Crary, M. Lu, L. Cheng, M. Palasis, R. L. Wilensky, A quantitative, randomized study evaluating three methods of mesenchymal stem cell delivery following myocardial infarction. *Eur. Heart J.* **27**, 1114–1122 (2006).
48. N. Nakagomi, T. Nakagomi, S. Kubo, A. Nakano-Doi, O. Saino, M. Takata, H. Yoshikawa, D. M. Stern, T. Matsuyama, A. Taguchi, Endothelial cells support survival, proliferation, and neuronal differentiation of transplanted adult ischemia-induced neural stem/progenitor cells after cerebral infarction. *Stem Cells* **27**, 2185–2195 (2009).
49. H. Toda, J. Takahashi, N. Iwakami, T. Kimura, S. Hoki, K. Mozumi-Kitamura, S. Ono, N. Hashimoto, Grafting neural stem cells improved the impaired spatial recognition in ischemic rats. *Neurosci. Lett.* **316**, 9–12 (2001).
50. N. Gupta, R. G. Henry, S. M. Kang, J. Strober, D. A. Lim, T. Ryan, R. Perry, J. Farrell, M. Ulman, R. Rajalingam, A. Gage, S. L. Huhn, A. J. Barkovich, D. H. Rowitch, Long-term safety, immunologic response, and imaging outcomes following neural stem cell transplantation for Pelizaeus-Merzbacher disease. *Stem. Cell Rep.* **13**, 254–261 (2019).
51. Y. Zheng, G. Wu, L. Chen, Y. Zhang, Y. Luo, Y. Zheng, F. Hu, T. Forouzanfar, H. Lin, B. Liu, Neuro-regenerative imidazole-functionalized GelMA hydrogel loaded with hAMSC and SDF-1 $\alpha$  promote stem cell differentiation and repair focal brain injury. *Bioact. Mater.* **6**, 627–637 (2021).
52. Y. Pei, L. Huang, T. Wang, Q. Yao, Y. Sun, Y. Zhang, X. Yang, J. Zhai, L. Qin, J. Xue, X. Wang, H. Zhang, J. Yan, Bone marrow mesenchymal stem cells loaded into hydrogel/nanofiber composite scaffolds ameliorate ischemic brain injury. *Mater. Today Adv.* **17**, 100349 (2023).
53. M. Alvarado-Velez, S. F. Enam, N. Mehta, J. G. Lyon, M. C. LaPlaca, R. V. Bellamkonda, Immuno-suppressive hydrogels enhance allogeneic MSC survival after transplantation in the injured brain. *Biomaterials* **266**, 120419 (2021).
54. S. Yao, F. He, Z. Cao, Z. Sun, Y. Chen, H. Zhao, X. Yu, X. Wang, Y. Yang, F. Rosei, L.-N. Wang, Mesenchymal stem cell-laden hydrogel microfibers for promoting nerve fiber regeneration in long-distance spinal cord transection injury. *ACS Biomater. Sci. Eng.* **6**, 1165–1175 (2020).
55. K. A. Tran, Y. Jin, J. Bouyer, B. J. DeOre, Ł. Suprewicz, A. Figel, H. Walens, I. Fischer, P. A. Galie, Magnetic alignment of injectable hydrogel scaffolds for spinal cord injury repair. *Biomater. Sci.* **10**, 2237–2247 (2022).
56. F. T. Afshari, J. C. Kwok, J. W. Fawcett, Astrocyte-produced ephrins inhibit schwann cell migration via VAV2 signaling. *J. Neurosci.* **30**, 4246–4255 (2010).
57. G. Jensen, J. L. Holloway, S. E. Stabenfeldt, Hyaluronic acid biomaterials for central nervous system regenerative medicine. *Cells* **9**, 2113 (2020).
58. X. B. Kong, Q. Y. Tang, X. Y. Chen, Y. Tu, S. Z. Sun, Z. L. Sun, Polyethylene glycol as a promising synthetic material for repair of spinal cord injury. *Neural Regen. Res.* **12**, 1003–1008 (2017).
59. T. F uhrmann, R. Y. Tam, B. Ballarin, B. Coles, I. Elliott Donaghue, D. van der Kooy, A. Nagy, C. H. Tator, C. M. Morshead, M. S. Shoichet, Injectable hydrogel promotes early survival of induced pluripotent stem cell-derived oligodendrocytes and attenuates long-term teratoma formation in a spinal cord injury model. *Biomaterials* **83**, 23–36 (2016).
60. S. D. Sommerfeld, J. H. Elisseff, Time to relax: Mechanical stress release guides stem cell responses. *Cell Stem Cell* **18**, 166–167 (2016).
61. C. Loebel, C. B. Rodell, M. H. Chen, J. A. Burdick, Shear-thinning and self-healing hydrogels as injectable therapeutics and for 3D-printing. *Nat. Protoc.* **12**, 1521–1541 (2017).
62. R. Milner, C. French-Constant, A developmental analysis of oligodendroglial integrins in primary cells: Changes in alpha v-associated beta subunits during differentiation. *Development* **120**, 3497–3506 (1994).
63. S. K. Seidlits, J. Liang, R. D. Bierman, A. Sohrabi, J. Karam, S. M. Holley, C. Cepeda, C. M. Walther, Peptide-modified, hyaluronic acid-based hydrogels as a 3D culture platform for neural stem/progenitor cell engineering. *J. Biomed. Mater. Res. A* **107**, 704–718 (2019).
64. W. Baron, S. J. Shattil, C. French-Constant, The oligodendrocyte precursor mitogen PDGF stimulates proliferation by activation of alpha(v)beta3 integrins. *EMBO J.* **21**, 1957–1966 (2002).
65. E. Ruoslahti, RGD and other recognition sequences for integrins. *Annu. Rev. Cell Dev. Biol.* **12**, 697–715 (1996).
66. B. Nasiri, T. Yi, Y. Wu, R. J. Smith Jr., A. K. Podder, C. K. Breuer, S. T. Andreadis, Monocyte recruitment for vascular tissue regeneration. *Adv. Healthc. Mater.* **n/a** **11**, e2200890 (2022).
67. A. K. Podder, M. A. Mohamed, G. Tseropoulos, B. Nasiri, S. T. Andreadis, Engineering nanofiber scaffolds with biomimetic cues for differentiation of skin-derived neural crest-like stem cells to Schwann cells. *Int. J. Mol. Sci.* **23**, 10834 (2022).
68. G. D. Conway, M. A. O'Bara, B. H. Vedia, S. U. Pol, F. J. Sim, Histone deacetylase activity is required for human oligodendrocyte progenitor differentiation. *Glia* **60**, 1944–1953 (2012).
69. S. U. Pol, J. K. Lang, M. A. O'Bara, T. R. Cimato, A. S. McCallion, F. J. Sim, Sox10-MCS5 enhancer dynamically tracks human oligodendrocyte progenitor fate. *Exp. Neurol.* **247**, 694–702 (2013).
70. R. R. Welliver, J. J. Polanco, R. A. Seidman, A. K. Sinha, M. A. O'Bara, Z. M. Khaku, D. A. Santiago Gonz alez, A. Nishiyama, J. Wess, M. L. Feltri, P. M. Paez, F. J. Sim, Muscarinic receptor M<sub>3</sub>R signaling prevents efficient remyelination by human and mouse oligodendrocyte progenitor cells. *J. Neurosci.* **38**, 6921–6932 (2018).
71. J. Wang, D. Saraswat, A. K. Sinha, J. Polanco, K. Dietz, M. A. O'Bara, S. U. Pol, H. J. Shayya, F. J. Sim, Paired related homeobox protein 1 regulates quiescence in human oligodendrocyte progenitors. *Cell Rep.* **25**, 3435–3450.e6 (2018).

#### Acknowledgments

**Funding:** This work was supported by NINDS grants R01NS130130 (S.T.A. and F.J.S.), R01NS104021 (F.J.S.), the Department of Defense Congressionally Directed Medical Research Programs W81XWH-21-1-0387 (F.J.S.), the Kaleic Multiple Sclerosis Foundation (F.J.S.), the Change MS Foundation (F.J.S.), and the New York Stem State Department of Health (Empire State Stem Cell Fund) through NYSTEM Contract #C30290GG (S.T.A.). J.J.P. was supported from NIGMS R25GM0954502 and NCATS UL1TR001412-S1. J.J.P. and R.A.S. received support from the New York State Department of Health (Empire State Stem Cell Fund) through the Stem Cells in Regenerative Medicine Fellowship NYSTEM C30290GG (S.T.A.). **Author contributions:** M.A.M., F.J.S., and S.T.A. conceived the project. A.K.P., M.A.M., F.J.S., and S.T.A. designed the research. F.J.S. and S.T.A. supervised the research. A.K.P. and M.A.M. performed and analyzed all experiments. A.K.P. and R.A.S. performed all animal surgeries with the help of G.T. and J.J.P. A.K.P. and P.L. cloned and expressed fusion peptides. M.A.M. designed, synthesized, characterized, and performed rheological measurements of all the materials of hydrogel with the help of A.K.P. A.K.P. performed and analyzed all cell culture experiments, tissue processing, immunofluorescence staining, and imaging of the samples with the help of R.A.S. and G.T. A.K.P., M.A.M., F.J.S., and S.T.A. wrote the manuscript. **Competing interests:** M.A.M. and S.T.A. are coauthors on a pending patent application describing the dynamic STH technology. The patent was filed by the University at Buffalo on 30 August 2022 under international application

number: PCT/US2022/042036 and published internationally on 09 March 2023 under international publication number: WO 2023/034299 A1. All other authors declare that they have no competing interests. **Data and materials availability:** All data needed to evaluate the conclusions in the paper are present in the paper and/or the Supplementary Materials.

Submitted 22 September 2023

Accepted 10 June 2024

Published 12 July 2024

10.1126/sciadv.adk9918